12. Niggli, V., Andréoli, C., Roy, C., and Mangeat, P. (1995) *FEBS Lett.* **376,** 172–176
13. Matsui, T., Maeda, M., Doi, Y., Yonemura, S., Amano, M., Kaibuchi, K., Tsukita, S., and Tsukita, S. (1998) *J. Cell Biol.* **140,** 647–657
14. Baumgartner, M., Sillman, A. L., Blackwood, E. M., Srivastava, J., Madson, N., Schilling, J. W., Wright, J. H., and Barber, D. L. (2006) *Proc. Natl. Acad. Sci. U.S.A.* **103,** 13391–13396
15. Ng, T., Parsons, M., Hughes, W. E., Monypenny, J., Zicha, D., Gautreau, A., Arpin, M., Gschmeissner, S., Verveer, P. J., Bastiaens, P. I., and Parker, P. J. (2001) *EMBO J.* **20,** 2723–2741
16. Koss, M., Pfeiffer, G. R., 2nd, Wang, Y., Thomas, S. T., Yerukhimovich, M., Gaarde, W. A., Doerschuk, C. M., and Wang, Q. (2006) *J. Immunol.* **176,** 1218–1227
17. Pasquale, E. B. (2010) *Nat. Rev. Cancer* **10,** 165–180
18. Surawska, H., Ma, P. C., and Salgia, R. (2004) *Cytokine Growth Factor Rev.* **15,** 419–433
19. Stein, E., Schoecklmann, H., and Daniel, T. O. (1997) *Trends Cardiovasc. Med.* **7,** 329–334
20. Miura, K., Nam, J. M., Kojima, C., Mochizuki, N., and Sabe, H. (2009) *Mol. Biol. Cell* **20,** 1949–1959
21. Martín-Villar, E., Megías, D., Castel, S., Yurrita, M. M., Vilaró, S., and Quintanilla, M. (2006) *J. Cell Sci.* **119,** 4541–4553
22. Martin-Belmonte, F., and Mostov, K. (2008) *Curr. Opin. Cell Biol.* **20,** 227–234
23. Ren, X. D., Kiosses, W. B., and Schwartz, M. A. (1999) *EMBO J.* **18,** 578–585
24. Yonemura, S., Matsui, T., Tsukita, S., and Tsukita, Sa. (2002) *J. Cell Sci.* **115,** 2569–2580
25. Crepaldi, T., Gautreau, A., Comoglio, P. M., Louvard, D., and Arpin, M. (1997) *J. Cell Biol.* **138,** 423–434
26. Zantek, N. D., Azimi, M., Fedor-Chaiken, M., Wang, B., Brackenbury, R., and Kinch, M. S. (1999) *Cell Growth Differ.* **10,** 629–638
27. Noren, N. K., Niessen, C. M., Gumbiner, B. M., and Burridge, K. (2001) *J. Biol. Chem.* **276,** 33305–33308
28. Noren, N. K., Arthur, W. T., and Burridge, K. (2003) *J. Biol. Chem.* **278,** 13615–13618
29. Arthur, W. T., Petch, L. A., and Burridge, K. (2000) *Curr. Biol.* **10,** 719–722
30. Honda, A., Nogami, M., Yokozeki, T., Yamazaki, M., Nakamura, H., Watanabe, H., Kawamoto, K., Nakayama, K., Morris, A. J., Frohman, M. A., and Kanaho, Y. (1999) *Cell* **99,** 521–532
31. Gabev, E., Kasianowicz, J., Abbott, T., and McLaughlin, S. (1989) *Biochim. Biophys. Acta* **979,** 105–112
32. Pujuguet, P., Del Maestro, L., Gautreau, A., Louvard, D., and Arpin, M. (2003) *Mol. Biol. Cell* **14,** 2181–2191
33. Dard, N., Louvet-Vallée, S., Santa-Maria, A., and Maro, B. (2004) *Dev. Biol.* **271,** 87–97
34. Saotome, I., Curto, M., and McClatchey, A. I. (2004) *Dev. Cell* **6,** 855–864
35. Kondo, T., Takeuchi, K., Doi, Y., Yonemura, S., Nagata, S., and Tsukita, S. (1997) *J. Cell Biol.* **139,** 749–758
36. Brown, M. J., Nijhara, R., Hallam, J. A., Gignac, M., Yamada, K. M., Erlandsen, S. L., Delon, J., Kruhlak, M., and Shaw, S. (2003) *Blood* **102,** 3890–3899
37. Delon, J., Kaibuchi, K., and Germain, R. N. (2001) *Immunity* **15,** 691–701
38. Gupta, N., Wollscheid, B., Watts, J. D., Scheer, B., Aebersold, R., and DeFranco, A. L. (2006) *Nat. Immunol.* **7,** 625–633
39. Zhuang, G., Hunter, S., Hwang, Y., and Chen, J. (2007) *J. Biol. Chem.* **282,** 2683–2694
40. Pandey, A., Lazar, D. F., Saltiel, A. R., and Dixit, V. M. (1994) *J. Biol. Chem.* **269,** 30154–30157
41. Brantley-Sieders, D. M., Caughron, J., Hicks, D., Pozzi, A., Ruiz, J. C., and Chen, J. (2004) *J. Cell Sci.* **117,** 2037–2049
42. Pilot, F., Philippe, J. M., Lemmers, C., and Lecuit, T. (2006) *Nature* **442,** 580–584

EphrinA/EphA signal facilitates insulin-like growth factor-I–induced myogenic differentiation through suppression of the Ras/extracellular signal–regulated kinase 1/2 cascade in myoblast cell lines

Masayoshi Minami[a], Tatsuya Koyama[a,b], Yuki Wakayama[a], Shigetomo Fukuhara[a], and Naoki Mochizuki[a]

[a]Department of Cell Biology, National Cerebral and Cardiovascular Center Research Institute, Osaka 565-8565, Japan; [b]Division of Cardiology, Department of Internal Medicine, Jikei University School of Medicine, Tokyo 105-8461, Japan

ABSTRACT **Insulin-like growth factor-I (IGF-I) activates not only the phosphatidylinositol 3-kinase (PI3K)–AKT cascade that is essential for myogenic differentiation but also the extracellular signal–regulated kinase (ERK) 1/2 cascade that inhibits myogenesis. We hypothesized that there must be a signal that inhibits ERK1/2 upon cell–cell contact required for skeletal myogenesis. Cell–cell contact–induced engagement of ephrin ligands and Eph receptors leads to downregulation of the Ras-ERK1/2 pathway through p120 Ras GTPase-activating protein (p120RasGAP). We therefore investigated the significance of the ephrin/Eph signal in IGF-I–induced myogenesis. EphrinA1-Fc suppressed IGF-I–induced activation of Ras and ERK1/2, but not that of AKT, in C2C12 myoblasts, whereas ephrinB1-Fc affected neither ERK1/2 nor AKT activated by IGF-I. IGF-I–dependent myogenic differentiation of C2C12 myoblasts was potentiated by ephrinA1-Fc. In p120RasGAP-depleted cells, ephrinA1-Fc failed to suppress the Ras-ERK1/2 cascade by IGF-I and to promote IGF-I–mediated myogenesis. EphrinA1-Fc did not promote IGF-I–dependent myogenesis when the ERK1/2 was constitutively activated. Furthermore, a dominant-negative EphA receptor blunted IGF-I–induced myogenesis in C2C12 and L6 myoblasts. However, the inhibition of IGF-I–mediated myogenesis by down-regulation of ephrinA/EphA signal was canceled by inactivation of the ERK1/2 pathway. Collectively, these findings demonstrate that the ephrinA/EphA signal facilitates IGF-I–induced myogenesis by suppressing the Ras-ERK1/2 cascade through p120RasGAP in myoblast cell lines.**

Monitoring Editor
Richard K. Assoian
University of Pennsylvania

Received: Mar 7, 2011
Revised: Jul 14, 2011
Accepted: Jul 21, 2011

This article was published online ahead of print in MBoC in Press (http://www.molbiolcell.org/cgi/doi/10.1091/mbc.E11-03-0183) on July 27, 2011.

Address correspondence to: Shigetomo Fukuhara (fuku@ri.ncvc.go.jp).

Abbreviations used: Ang1, angiopoietin-1; β-gal, β-galactosidase; bFGF, basic fibroblast growth factor; caMEK1, constitutively active form of MEK1; COMP, cartilage oligomeric matrix protein; EphA2Δcyto, EphA2 mutant that lacks the cytoplasmic region; ERK, extracellular signal–regulated kinase; FBS, fetal bovine serum; Ig, immunoglobulin; IGF, insulin-like growth factor; MAPK, mitogen-activated protein kinase; MEK1/2, MAPK/ERK kinase1/2; MHC, myosin heavy chain; p120RasGAP, p120 Ras GTPase-activating protein; PI3K, phosphatidylinositol 3-kinase; RTK, receptor tyrosine kinase; siRNA, small interfering RNA.

INTRODUCTION

Skeletal myogenesis is a complex process that begins with the commitment of multipotent mesodermal precursor cells to the muscle fate (Andres and Walsh, 1996; Taylor, 2002). These committed cells—the myoblasts—subsequently withdraw from the cell cycle, differentiate, and fuse into multinucleated myotubes. In culture, most skeletal muscle cell lines proliferate under high serum conditions, whereas the cells placed under low serum conditions spontaneously undergo differentiation into myotubes (Florini *et al.*, 1991; Ewton *et al.*, 1994; Bach *et al.*, 1995).

Differentiation of skeletal muscle cells is positively and negatively regulated by two major intracellular signaling pathways, namely the phosphatidylinositol 3-kinase (PI3K)–AKT cascade and the extracellular signal–regulated kinase (ERK) 1/2 cascade (Kaliman *et al.*, 1996,

1998; Bennett and Tonks, 1997; Coolican *et al.*, 1997; Tortorella *et al.*, 2001; de Alvaro *et al.*, 2005; Koyama *et al.*, 2008). The latter involves Ras, Raf, mitogen-activated protein kinase (MAPK)/ERK kinase1/2 (MEK1/2), and ERK1/2. Activation of ERK1/2 cascade evoked by mitogens induces proliferation of cultured skeletal muscle cells but prevents their differentiation (Bennett and Tonks, 1997; Coolican *et al.*, 1997; Tortorella *et al.*, 2001; de Alvaro *et al.*, 2005; Koyama *et al.*, 2008). Among various growth factors, the insulin-like growth factors (IGFs), including IGF-I and IGF-II, have been reported to be quite singular, in that they stimulate both proliferation and differentiation of muscle cells in culture (Florini *et al.*, 1991, 1996; Coolican *et al.*, 1997; Kaliman *et al.*, 1998; Koyama *et al.*, 2008; Clemmons, 2009).

IGF-I receptor, which belongs to receptor tyrosine kinase (RTK) family, activates the PI3K–AKT signaling cascade in response to IGFs, thereby promoting differentiation of skeletal muscle cells (Florini *et al.*, 1996; Coolican *et al.*, 1997; Kaliman *et al.*, 1998; White, 2003). The importance of the IGF/IGF-I receptor signal in muscle development is also illustrated by the poor muscle development and dystrophic phenotype of IGF-I receptor–deficient mice (Liu *et al.*, 1993). However, the IGF/IGF-I receptor signal also induces activation of ERK1/2 through Grb2-associated binder 1–SHP2 signaling pathways in C2C12 cells, which counteracts PI3K/AKT signal-mediated myogenic differentiation (Coolican *et al.*, 1997; Koyama *et al.*, 2008). Thus the differentiation of myoblasts into myotubes is determined by the balance between the positive and negative signals mediated through PI3K–AKT and ERK1/2 cascades, respectively.

Myoblast differentiation is regulated not only by the signaling pathways induced by soluble myogenic growth factors but also by those initiated by cell–cell contacts (Krauss, 2010; Pavlath, 2010). Cell–cell adhesions are constituted by cadherin and other junctional molecules. Among them, N-cadherin (also known as cadherin-2) is expressed throughout skeletal myogenesis and was shown to be involved in myogenic differentiation in myoblast cell lines (Charrasse *et al.*, 2002; Gavard *et al.*, 2004; Lovett *et al.*, 2006; Krauss, 2010). N-cadherin associates in *cis* with Cdo, a cell surface receptor of the immunoglobulin (Ig) superfamily in C2C12 myoblasts (Lu and Krauss, 2010). On N-cadherin ligation, the Cdo intracellular region binds to Bnip-2, a scaffold protein for Cdc42 small GTPase, and to JLP, a scaffold protein for the p38α/β MAPK, which results in Cdc42-dependent activation of p38α/β (Takaesu *et al.*, 2006; Kang *et al.*, 2008). In contrast to ERK1/2 MAPK, the p38α/β pathway promotes skeletal myogenesis by inducing the expression of muscle-specific genes in myoblast cell lines and primary myoblasts (Guasconi and Puri, 2009). Thus, upon cell–cell contact formation, the N-cadherin/Cdo complex promotes myogenic differentiation through activation of the p38α/β pathway. N-cadherin engagement also induces activation of RhoA, leading to serum response factor–dependent expression of muscle-specific genes in skeletal muscle cell lines (Carnac *et al.*, 1998). It has also been suggested that M-cadherin, another member of the classic cadherin family, regulates myoblast fusion through Trio guanine nucleotide exchange factor–dependent activation of Rac1 in C2C12 myoblasts (Charrasse *et al.*, 2007). In addition to cadherins, Ig superfamily members such as neogenin and neural cell adhesion molecule also regulate myogenic differentiation of cultured myoblasts in a cell–cell contact–dependent manner (Kang *et al.*, 2004; Krauss, 2010). These results reveal the importance of the signaling pathways mediated by cell–cell contacts for myoblast differentiation.

Eph receptors and their ligands—ephrins—constitute the largest subfamily of RTKs, and have been implicated in diverse physiological and pathophysiological functions, such as neural development, angiogenesis, and tumorigenesis (Pasquale, 2005, 2008). The Eph receptors are divided into two classes, EphA and EphB, based on their ability to bind the ligands ephrinA and ephrinB, respectively. Unlike other RTK ligands, both ephrinA and ephrinB are membrane-bound proteins (Pasquale, 2005, 2008). EphrinAs anchor to the plasma membrane via a glycosylphosphatidylinositol moiety, whereas ephrinBs contain a transmembrane domain. Thus ephrin/Eph signaling is initiated by the formation of cell–cell contacts (Pasquale, 2010). On ephrin binding, Eph receptors undergo autophosphorylation at tyrosine residues in the cytoplasmic domain, which then triggers downstream signaling cascades through interaction with several signaling molecules, including p120 Ras GTPase-activating protein (p120RasGAP) (Pasquale, 2010). It has been shown that the ephrin/Eph signal negatively regulates the Ras-ERK1/2 cascade through inhibition of Ras by p120RasGAP in various types of cell lines (Elowe *et al.*, 2001; Miao *et al.*, 2001; Tong *et al.*, 2003; Parri *et al.*, 2005; Pasquale, 2010). The evidence that the Eph/ephrin signal depends on cell–cell contacts and its ability to down-regulate the Ras-ERK1/2 cascade prompted us to test our hypothesis that the ephrin/Eph signal promotes myogenic differentiation by reducing the myogenic inhibitory signal mediated by the Ras-ERK1/2 cascade. In this study, we found that the cell–cell contact–dependent ephrinA/EphA signal down-regulates the IGF-I–induced ERK1/2 pathway through p120RasGAP in myoblast cell lines, thereby accelerating myogenic differentiation.

RESULTS

EphrinA/EphA signal represses IGF-I–induced activation of ERK1/2, but not AKT, through p120RasGAP in mouse C2C12 and rat L6 myoblasts

To investigate whether the ephrin/Eph signal downregulates the Ras-ERK1/2 cascade in myoblasts, we examined the effect of ephrinA1-Fc or ephrinB1-Fc on IGF-I–induced activation of ERK1/2 and AKT in myoblast cell lines. IGF-I induced activation of both ERK1/2 and AKT in sparse cultures of mouse C2C12 and rat L6 cells (Figure 1 and Supplemental Figure S1, A and B). EphrinA1-Fc, but not Fc, dramatically suppressed IGF-I–induced activation of ERK1/2 (Figure 1 and Supplemental Figure S1, A and B). In clear contrast, IGF-I–induced activation of AKT was unaffected by ephrinA1-Fc (Figure 1 and Supplemental Figure S1, A and B). EphrinB1-Fc did not affect IGF-I–induced activation of ERK1/2 and AKT in C2C12 cells (Supplemental Figure S1C). To confirm that ephrinB1-Fc used in this experiment is functional, we also examined the effect of ephrinB1-Fc on activation of ERK1/2 by cartilage oligomeric matrix protein (COMP)–angiopoietin-1 (Ang1), a potent Ang1 variant, in human umbilical vein endothelial cells, since it was reported that the ephrinB/EphB signal suppresses Ang1-induced activation of ERK1/2 in endothelial cells (Kim *et al.*, 2002). COMP-Ang1–induced activation of ERK1/2 was clearly attenuated by the treatment with ephrinB1-Fc (Supplemental Figure S1D). These results indicate that the ephrinA/EphA signal, but not the ephrinB/EphB signal, downregulates the IGF-I–induced ERK1/2 cascade without affecting the AKT activation by IGF-I in C2C12 and L6 myoblasts.

It is known that p120RasGAP is recruited to the ephrinA-stimulated EphA receptors, leading to down-regulation of the Ras–ERK1/2 pathway (Pasquale, 2010). Thus we next investigated whether the ephrinA/EphA signal down-regulates the IGF-I–induced ERK1/2 cascade by decreasing Ras activity through p120RasGAP. IGF-I induced activation of Ras in C2C12 myoblasts (Figure 2A). IGF-1–induced Ras activation was suppressed by ephrinA1-Fc (Figure 2A). However, ephrinA1-Fc failed to suppress the IGF-I–induced Ras activation when p120RasGAP was depleted by small interfering RNAs

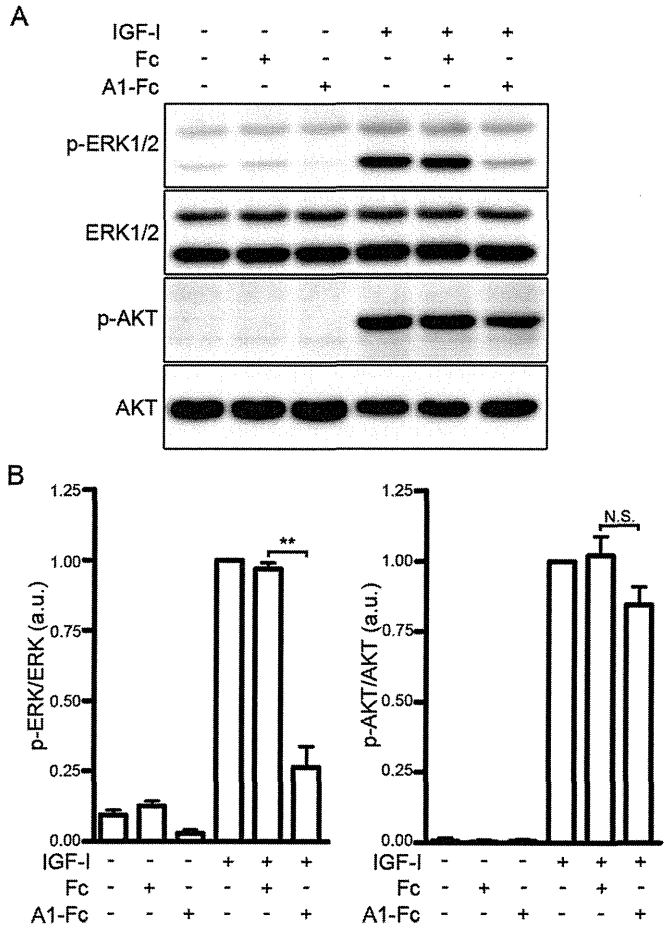

FIGURE 1: The ephrinA/EphA signal suppresses IGF-I–induced activation of ERK1/2 in C2C12 myoblasts. (A) Serum-starved C2C12 myoblasts were stimulated for 10 min with or without 10 nM IGF-I in the presence or absence of 1.7 nM Fc (Fc) or ephrinA1-Fc (A1-Fc) as indicated at the top. Cell lysates were subjected to Western blot analysis with anti–phospho-ERK1/2 (p-ERK1/2), anti-ERK1/2 (ERK1/2), anti–phospho-AKT (p-AKT), and anti-AKT (AKT) antibodies as indicated at the left. (B) Phosphorylation levels of ERK1/2 (left) and AKT (right) observed in A were quantified and represented by the ratio of phospho-ERK1/2 or phospho-AKT to total ERK1/2 or total AKT, respectively. The value for each group is expressed relative to the ratio observed in the cells stimulated with IGF-I in the absence of Fc and ephrinA1-Fc and shown as means ± SD of three independent experiments. **$p < 0.01$, significant difference between two groups. N.S., no significance between two groups. a.u., arbitrary unit(s).

(siRNAs; Figure 2A). Consistently, depletion of p120RasGAP by siRNA blunted the inhibitory effect of ephrinA1-Fc on IGF-I–induced activation of ERK1/2, although it had no effect on IGF-I–induced activation of ERK1/2 and AKT (Figure 2, B and C). Collectively, these findings indicate that the ephrinA/EphA signal downregulates the IGF-I–evoked Ras–ERK1/2 cascade through p120RasGAP in C2C12 myoblasts.

EphrinA/EphA signal enhances IGF-I–induced myogenic differentiation

Myogenic differentiation is negatively and positively regulated by the ERK1/2 and AKT cascades, respectively (Kaliman *et al.*, 1996, 1998; Bennett and Tonks, 1997; Coolican *et al.*, 1997; Tortorella *et al.*, 2001; de Alvaro *et al.*, 2005; Koyama *et al.*, 2008). Because the ephrinA/EphA signal downregulates the ERK1/2 cascade without affecting the AKT pathway in myoblast cell lines, we hypothesized that myogenic differentiation might be enhanced by the ephrinA/EphA signal. To address this possibility, confluent C2C12 myoblasts were differentiated into myotubes by being incubated in DMEM containing 1% fetal bovine serum (FBS) and 10 nM IGF-I in the presence of either Fc or ephrinA1-Fc. To evaluate myogenic differentiation, the expression of muscle-specific myosin heavy chain (MHC) protein was examined by immunocytochemical and Western blot analyses. On the third day after induction of myogenic differentiation, formation of MHC-positive myotubes was greater in the cells differentiated in the presence of ephrinA1-Fc than in those in the presence of Fc (control; Figure 3, A and B). Consistently, expression of MHC protein was 2.4 and 1.6 times higher in the ephrinA1-Fc–treated cells than in those treated with Fc on the second and third days after induction of differentiation, respectively (Figure 3, C and D). Similarly, myogenic differentiation of C2C12 cells induced by low concentrations of IGF-I was also potentiated by the treatment with ephrinA1-Fc (Supplemental Figure S2). These results indicate that activation of the ephrinA/EphA signal results in enhancement of IGF-I–dependent myogenic differentiation in C2C12 cells.

EphrinA/EphA signal promotes IGF-I–induced myogenic differentiation by suppressing the Ras–ERK1/2 cascade through p120RasGAP

To investigate whether the ephrinA/EphA signal promotes IGF-I–dependent myogenic differentiation by suppressing the Ras–ERK1/2 pathway through p120RasGAP, we examined the effect of p120RasGAP depletion on the enhancement of IGF-I–induced myogenic differentiation by the ephrinA/EphA signal. C2C12 myoblasts transfected with either control siRNA or two independent siRNAs targeting p120RasGAP were differentiated in the media containing both IGF-I and ephrinA1-Fc for 2 d. Myogenic differentiation of C2C12 cells was significantly suppressed in the p120RasGAP-depleted cells compared to the cells transfected with control siRNA, as assessed by immunocytochemical analysis with anti-MHC antibody (Figure 4, A and B). Consistently, the expression of MHC was decreased by the depletion of p120RasGAP (Figure 4, C and D). These findings show that the ephrinA/EphA signal implicates p120RasGAP in the enhancement of the IGF-I–induced myogenic differentiation of C2C12 cells.

To further clarify whether the ephrinA/EphA signal promotes IGF-I–dependent myogenic differentiation through inactivation of ERK1/2 pathway, we examined the effect of adenovirus-mediated overexpression of a constitutively active mutant of MEK1 (caMEK1). As expected, overexpression of caMEK1 in C2C12 cells resulted in constitutive activation of ERK1/2 (Figure 5A). Inactivation of ERK1/2 in response to IGF-I by ephrinA1-Fc was canceled in the cells expressing caMEK1, although overexpression of caMEK1 did not affect IGF-I–induced AKT activation in the presence or absence of ephrinA1-Fc (Figure 5A). In the C2C12 myoblasts expressing caMEK1, IGF-I failed to induce formation of MHC-positive myotubes even in the presence of ephrinA1-Fc (Figure 5, B and C). Consistently, IGF-I–induced expression of MHC was prevented by overexpression of caMEK1 irrespective of the presence or absence of ephrinA1-Fc (Figure 5, D and E). Collectively, these findings indicate that the ephrinA/EphA signal potentiates IGF-I–induced myogenic differentiation of C2C12 cells through p120RasGAP-mediated down-regulation of the Ras–ERK1/2 cascade.

EphA2 receptor that lacks the cytoplasmic domain acts as a dominant-negative mutant for EphA family members

We further investigated whether the ephrinA/EphA signal is required for IGF-I–dependent myogenic differentiation. Because reverse

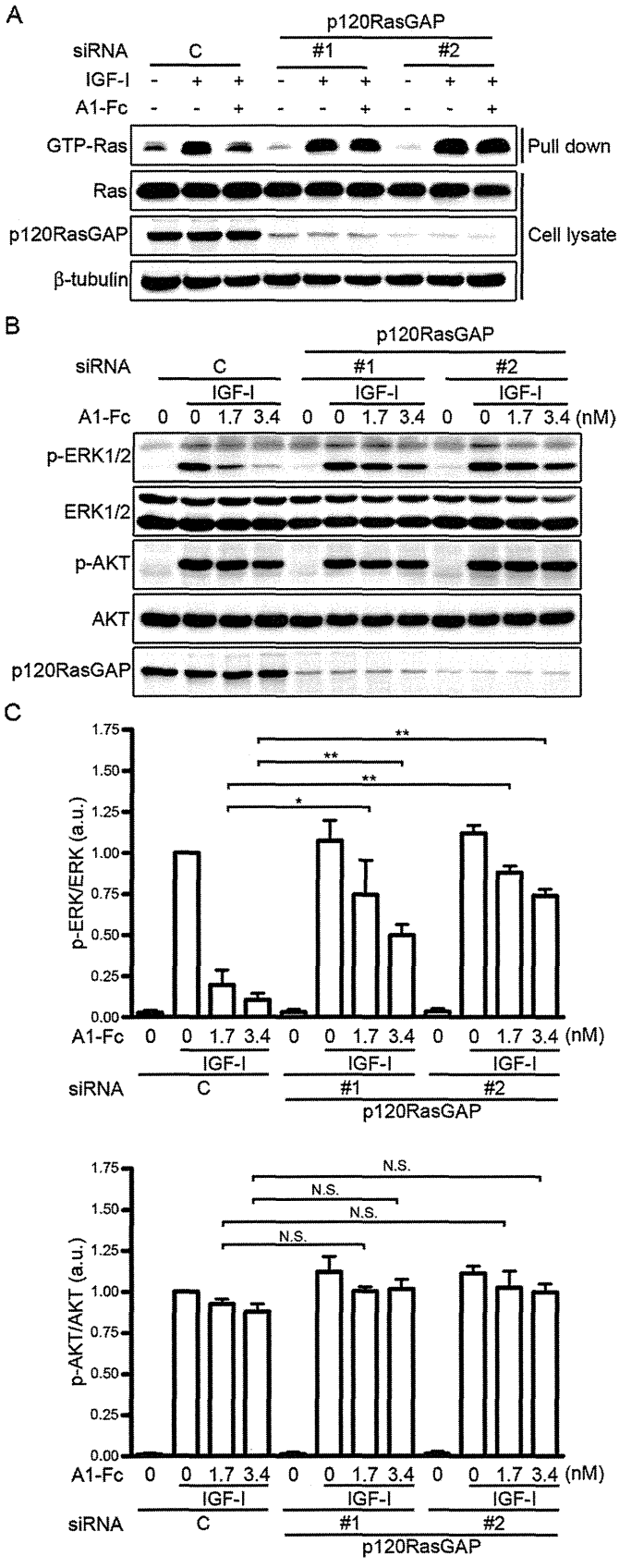

FIGURE 2: The ephrinA/EphA signal suppresses the IGF-I–induced Ras–ERK1/2 pathway through p120RasGAP. (A) Serum-starved C2C12 myoblasts transfected with either control siRNA (C) or two independent siRNAs targeting p120RasGAP (1 and 2) were stimulated for 5 min with or without 10 nM IGF-1 in the absence (–) or presence (+) of 1.7 nM ephrinA1-Fc (A1-Fc) as indicated at the top. GTP-bound Ras was collected as described in *Materials and Methods* and subjected to Western blot analysis with anti-Ras antibody (GTP-Ras). Aliquots of cell lysates were also subjected to Western blot analysis with anti-Ras (Ras), anti-p120RasGAP (p120RasGAP), and anti–β-tubulin (β-tubulin) antibodies as indicated at the left. (B) Serum-starved C2C12 myoblasts transfected with siRNA as described in A were stimulated for 10 min with or without 10 nM IGF-I in the absence or presence of 1.7 or 3.4 nM ephrinA1-Fc (A1-Fc) as indicated at the top. Cell lysates were subjected to Western blot analysis with anti–phospho-ERK1/2 (p-ERK1/2), anti-ERK1/2 (ERK1/2), anti–phospho-AKT (p-AKT), anti-AKT (AKT), and anti-p120RasGAP (p120RasGAP) antibodies as indicated at the left. (C) Phosphorylation levels of ERK1/2 (top) and AKT (bottom) observed in B were quantified and represented by the ratio of phospho-ERK1/2 or phospho-AKT to total ERK1/2 or total AKT, respectively. Values are expressed as explained in the legend of Figure 1B. Values are expressed relative to the ratio obtained from the IGF-I–treated cells transfected with control siRNA. *$p < 0.05$, **$p < 0.01$, significant differences between two groups. N.S., no significance between two groups. a.u., arbitrary unit(s).

transcription (RT)–PCR analysis revealed that C2C12 myoblasts express multiple members of ephrinA ligands such as ephrinA1, ephrinA3, ephrinA4, and ephrinA5 and those of EphA receptors, which include EphA1, EphA2, EphA3, and EphA4 (Supplemental Figure S3), we decided to use a dominant-negative approach instead of performing siRNA-mediated silencing of ephrinA ligands and EphA receptors. We prepared the adenovirus encoding the EphA2 receptor mutant lacking the cytoplasmic region (EphA2Δcyto), which was previously reported to exhibit dominant-negative activity (Cheng *et al.*, 2003; Taddei *et al.*, 2009). Overexpression of EphA2Δcyto blunted the ephrinA1-Fc–mediated phosphorylation of EphA2 in C2C12 cells (Figure 6A). It is significant that phosphorylation of EphA2 was greater in the confluent C2C12 cells than in the sparse cells (Figure 6B). Phosphorylation of EphA2 was likely to be induced by the binding of EphA2 to endogenous ephrinA upon cell–cell contact. EphA2 phosphorylation observed in the confluent cells was decreased by overexpression of EphA2Δcyto (Figure 6B), indicating that the EphA2 signal functions under confluent culture conditions and can be blocked by overexpression of EphA2Δcyto. Because C2C12 cells express several members of the EphA receptor family, as indicated by RT-PCR analysis, it can be assumed that ephrinA1-Fc suppresses IGF-I–induced activation of ERK1/2 through multiple members of EphA receptors. In C2C12 and L6 myoblasts, the inhibitory effect of ephrinA1-Fc on ERK1/2 activation in response to IGF-I was canceled by overexpression of EphA2Δcyto (Figure 6C and Supplemental Figure S4), implying that EphA2Δcyto acts as a dominant-negative mutant not only for EphA2, but also for other members of the EphA receptor family.

Endogenous ephrinA/EphA signal is required for efficient myogenic differentiation induced by IGF-I

To clarify the role of the ephrinA/EphA signal in IGF-I–induced myogenic differentiation, the EphA signal was abrogated by EphA2Δcyto overexpression during IGF-I–induced myogenic differentiation. C2C12 and L6 myoblasts infected with adenoviruses encoding EphA2Δcyto exhibited decreased formation of MHC-positive myotubes compared to the uninfected cells or the cells infected with β-galactosidase (β-gal)–encoding adenoviruses (Figure 7, A and B, and Supplemental Figure S5A). Consistently, IGF-I–mediated expression of MHC protein was significantly reduced by EphA2Δcyto overexpression (Figure 7, C and D, and Supplemental Figure S5B).

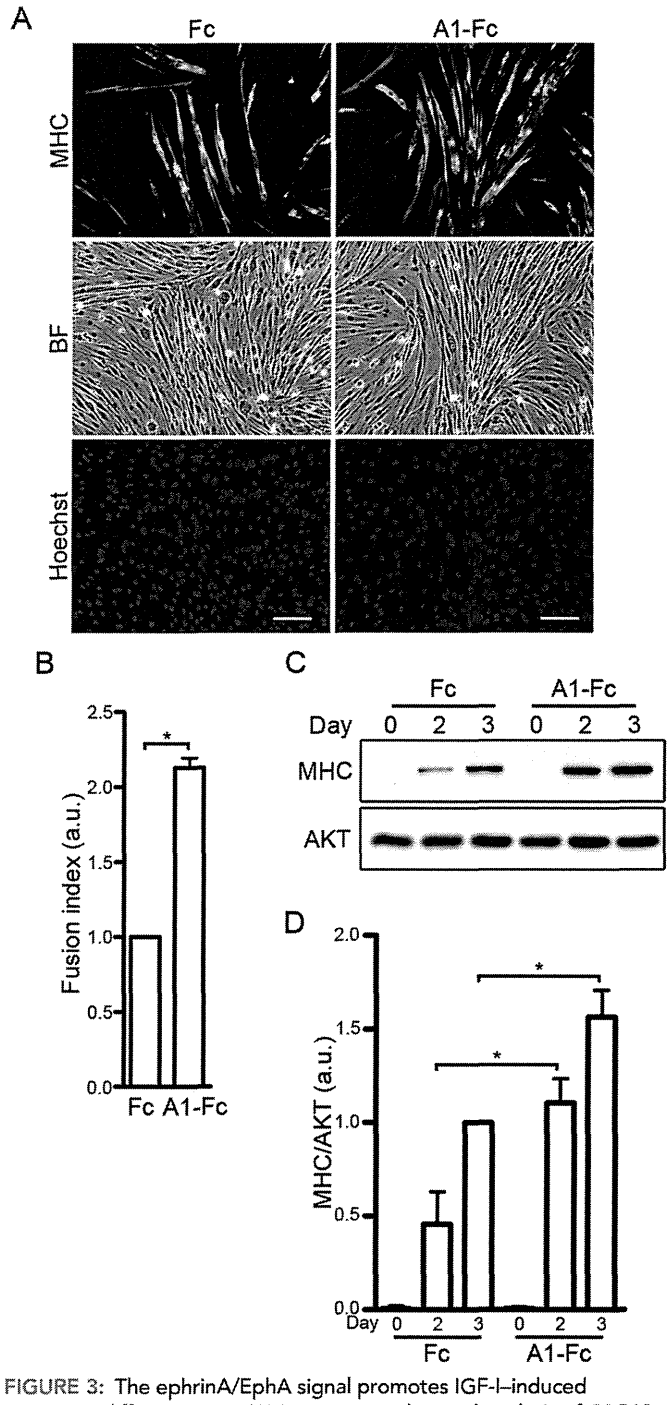

FIGURE 3: The ephrinA/EphA signal promotes IGF-I–induced myogenic differentiation. (A) Immunocytochemical analysis of C2C12 myoblasts using anti-MHC antibody. Confluent cells were differentiated into myotubes in DMEM containing 1% FBS and 10 nM IGF-I in the presence of either 6.4 nM Fc (Fc) or ephrinA1-Fc (A1-Fc) for 3 d. The cells were then fixed, immunostained with anti-MHC antibody, and visualized with Alexa Fluor 488–conjugated secondary antibody. The cells were also poststained with Hoechst 33342 to visualize the nuclei. Alexa 488 (MHC), bright-field (BF), and Hoechst 33342 (Hoechst) images are shown as indicated at the left. Experiments were repeated three times with similar results. Scale bars, 100 μm. (B) The fusion index observed in A was determined by dividing the number of nuclei within multinucleated myotubes by the total number of nuclei analyzed. Values are expressed relative to that observed in the cells differentiated in the presence of Fc and shown as means ± SD of three independent experiments. (C) Confluent C2C12 myoblasts were differentiated into myotubes in DMEM containing 1% FBS and 10 nM IGF-I in the presence of either 6.4 nM Fc (Fc) or ephrinA1-Fc (A1-Fc) for time periods (days) indicated at the top. Cell lysates were subjected to Western blot analysis using anti-MHC (MHC) and anti-AKT (AKT) antibodies as indicated at the left. (D) The expression level of MHC observed in C was quantified by normalizing the expression of MHC by that of AKT. Values are expressed relative to that observed in the cells differentiated in the presence of Fc for 3 d and shown as means ± SD of three independent experiments. *$p < 0.05$, significant differences between two groups. a.u., arbitrary unit(s).

These findings indicate that the ephrinA/EphA signal is required for efficient myogenic differentiation induced by IGF-I in myoblast cell lines.

To investigate whether myogenic differentiation induced by IGF-I requires the suppression of ERK1/2 activity by the ephrinA/EphA signal, we first examined the effect of EphA2Δcyto overexpression on ERK1/2 activity by inducing differentiation with IGF-I. The ERK1/2 activity of the C2C12 cells expressing EphA2Δcyto varied at the several time points during differentiation and was not always significantly increased compared with either the parental cells or those expressing β-gal. Therefore, to further assess the effect of EphA2Δcyto on the ERK1/2 activity during the differentiation, we examined it using the cells in the presence of ephrinA1-Fc in addition to IGF-1. C2C12 cells infected with adenoviruses expressing EphA2Δcyto exhibited a high level of ERK1/2 activity compared to those infected without or with β-gal–expressing adenoviruses during myogenic differentiation (Supplemental Figure S6). Furthermore, we investigated the effect of a MEK1/2 inhibitor, U0126, on the IGF-I–induced myogenic differentiation. U0126 slightly enhanced formation of MHC-positive myotubes and increased the expression of MHC in C2C12 and L6 myoblasts infected with or without β-gal–encoding adenoviruses (Figure 8 and Supplemental Figure S5). As observed in Figure 7, overexpression of EphA2Δcyto partially inhibited myotube formation and decreased the expression of MHC (Figure 8 and Supplemental Figure S5). However, the inhibitory effect of EphA2Δcyto on IGF-I-mediated myogenic differentiation was completely suppressed by the treatment with U0126 (Figure 8 and Supplemental Figure S5). Collectively, these findings suggest that IGF-I–induced myogenic differentiation is facilitated by the ephrinA/EphA signal, leading to down-regulation of the ERK1/2 cascade in myoblast cell lines.

DISCUSSION

In the present study, we investigated the role of ephrin/Eph signaling in skeletal muscle differentiation and found that the ephrinA/EphA signal facilitates IGF-I–induced myogenic differentiation by repressing the Ras–ERK1/2 signaling cascade through p120RasGAP in myoblast cell lines (Figure 9). To our knowledge, this study reveals for the first time the potential role of the ephrinA/EphA signal in skeletal myogenesis.

We delineated the molecular mechanism by which an endogenous ephrinA/EphA signal is involved in the inactivation of ERK1/2 that is preferable for myogenic differentiation induced by IGF-I. Although it is well known that IGFs promote myogenic differentiation through the PI3K/AKT pathway, IGFs also induces activation of myogenic inhibitory signal mediated by the ERK1/2. Activation of the PI3K/AKT pathway is responsible for myogenic differentiation, whereas the ERK1/2 pathway counteracts the PI3K/AKT pathway–dependent myogenic differentiation (Kaliman *et al.*, 1996, 1998; Bennett and Tonks, 1997; Coolican *et al.*, 1997; Tortorella *et al.*,

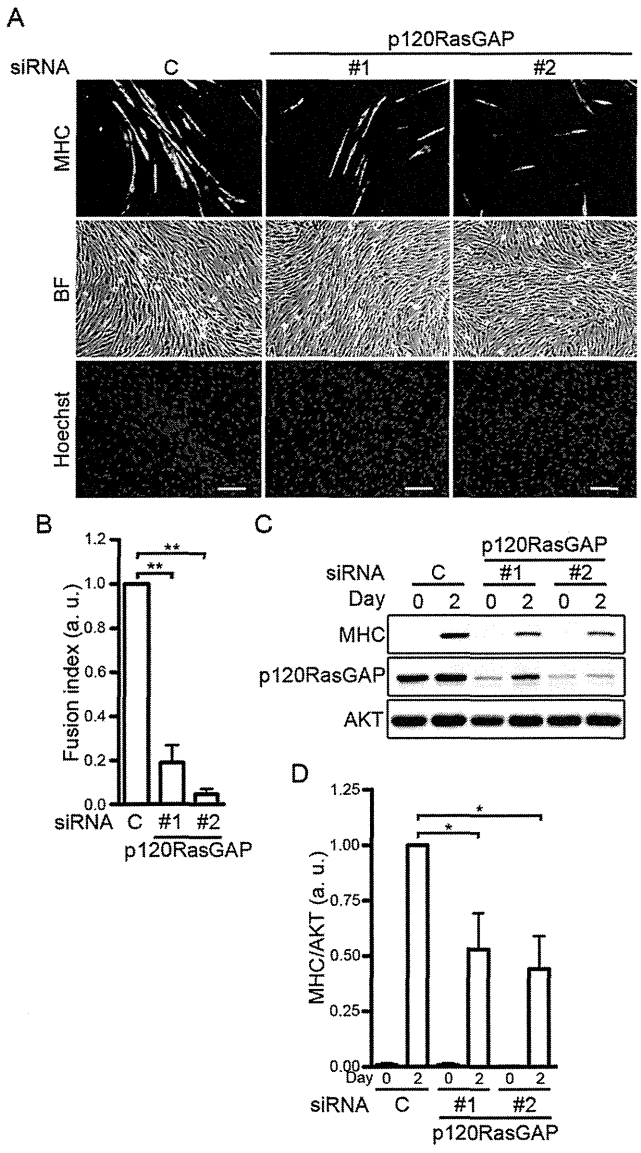

FIGURE 4: The ephrinA/EphA signal promotes IGF-I–dependent myogenic differentiation through p120RasGAP. (A) C2C12 myoblasts transfected with either control siRNA (C) or two independent siRNAs targeting p120RasGAP (1 and 2) were differentiated into myotubes in DMEM containing 1% FBS and 10 nM IGF-I in the presence of 6.4 nM ephrinA1-Fc for 2 d. The cells were immunostained with anti-MHC antibody and visualized with Alexa Fluor 488–conjugated secondary antibody. The cells were also poststained with Hoechst 33342 to visualize the nuclei. Alexa 488 (MHC), bright-field (BF), and Hoechst 33342 (Hoechst) images are shown as indicated at the left. Experiments were repeated three times with similar results. Scale bars, 100 μm. (B) The fusion index observed in A was determined as described in the legend of Figure 3B. Values are expressed relative to that observed in the cells transfected with control siRNA and shown as means ± SD of three independent experiments. (C) siRNA-transfected C2C12 myoblasts were differentiated into myotubes as described in A for time periods (days) indicated at the top. Cell lysates were subjected to Western blot analysis using anti-MHC (MHC), anti-p120RasGAP (p120RasGAP), and anti-AKT (AKT) antibodies as indicated at the left. (D) Expression level of MHC observed in C was quantified by normalizing the expression of MHC by that of AKT. Values are expressed relative to that observed in the control siRNA-transfected cells differentiated for 2 d and shown as means ± SD of three independent experiments. *$p < 0.05$, **$p < 0.01$, significant differences between two groups. a.u., arbitrary unit(s).

2001; de Alvaro *et al.*, 2005; Koyama *et al.*, 2008). Thus it is reasonable that the mechanisms that suppress the ERK1/2 pathway might exist to facilitate myogenic differentiation during skeletal myogenesis.

The EphrinA/EphA signal in C2C12 cells suppresses ERK1/2 during myogenesis. EphA and EphB receptors inhibit the Ras–ERK1/2 pathway by decreasing the Ras activity through p120RasGAP in various types of cells (Elowe *et al.*, 2001; Miao *et al.*, 2001; Tong *et al.*, 2003; Parri *et al.*, 2005; Pasquale, 2010). Thus, we assumed that the ephrin/Eph signal is favorable for skeletal myogenesis and found that the ephrinA/EphA signal down-regulates the Ras–ERK1/2 pathway induced by IGF-I through p120RasGAP in myoblast cell lines, thereby facilitating myogenic differentiation. In addition, it was previously reported that DA-Raf1, a splicing isoform of A-Raf, is expressed during skeletal myogenesis and enhances myogenic differentiation of C2C12 cells by acting as a dominant-negative antagonist of the Ras–ERK1/2 pathway (Yokoyama *et al.*, 2007). Recently glypican, a heparin sulfate proteoglycan expressed in myoblasts, was reported to sequester basic fibroblast growth factor (bFGF) in lipid rafts away from its receptors (Gutierrez and Brandan, 2010). Because bFGF represses myogenic differentiation through the activation of the ERK1/2 pathway (Tortorella *et al.*, 2001), sequestration of bFGF by glypican promotes myogenic differentiation. Therefore the ERK1/2 activity in myoblasts is suppressed by various mechanisms to facilitate myogenic differentiation during skeletal myogenesis.

Temporal ERK1/2 inactivation and activation might be important for myogenesis. The ERK1/2 cascade is essential for proliferation of myoblasts but negatively regulates myogenic differentiation by suppressing the expression of muscle-specific genes. Of interest, it was also shown that the late stage of skeletal muscle differentiation requires the ERK1/2 activity (Bennett and Tonks, 1997). Expression of MAPK phosphatase-1, which inhibits ERK1/2 activity, is down-regulated during the late stage of myogenesis, and its overexpression prevents myotube formation without affecting the expression of muscle-specific genes. Thus the ERK1/2 activity is temporarily controlled during myogenic differentiation. On induction of myogenic differentiation, the cell–cell contact–dependent ephrinA/EphA signal suppresses ERK1/2 activity, as we demonstrated in this study. However, the ephrinA/EphA signal may be down-regulated to reactivate the ERK1/2 cascade at the late stage of skeletal muscle differentiation. Because EphA2 expression is induced by activation of the Ras–ERK1/2 pathway (Macrae *et al.*, 2005), EphA-signal–dependent inhibition of the Ras–ERK1/2 pathway may lead to down-regulation of EphA2 expression. Therefore the ERK1/2 activity may be temporarily controlled by an EphA2–Ras–ERK1/2 negative feedback loop during skeletal myogenesis.

There is only limited information on the role of the ephrin/Eph signal in muscle development. It was shown that the ephrinA5/EphA4 signal is involved in migration of muscle precursor cells (Swartz *et al.*, 2001). EphrinA5 expressed in mesoderm tissue prevents EphA4-positive muscle precursor cells from migrating into abnormal embryonic regions. Furthermore, a role of EphA4 signal in maintenance of neuromuscular junctions was suggested (Lai *et al.*, 2004). EphA4 localized at the neuromuscular junctions of adult muscle induces expression of acetylcholinesterase, an enzyme that degrades the neurotransmitter acetylcholine, through Janus kinase/signal transducers and activators of transcription pathway. However, the role of ephrin/Eph signal in differentiation of myoblasts into myocytes has never been reported. Therefore the present study is the first to unravel the potential role of the ephrinA/EphA signal in myogenic differentiation of myoblast cell lines. However, further study is required to clarify whether the ephrinA/EphA signal is

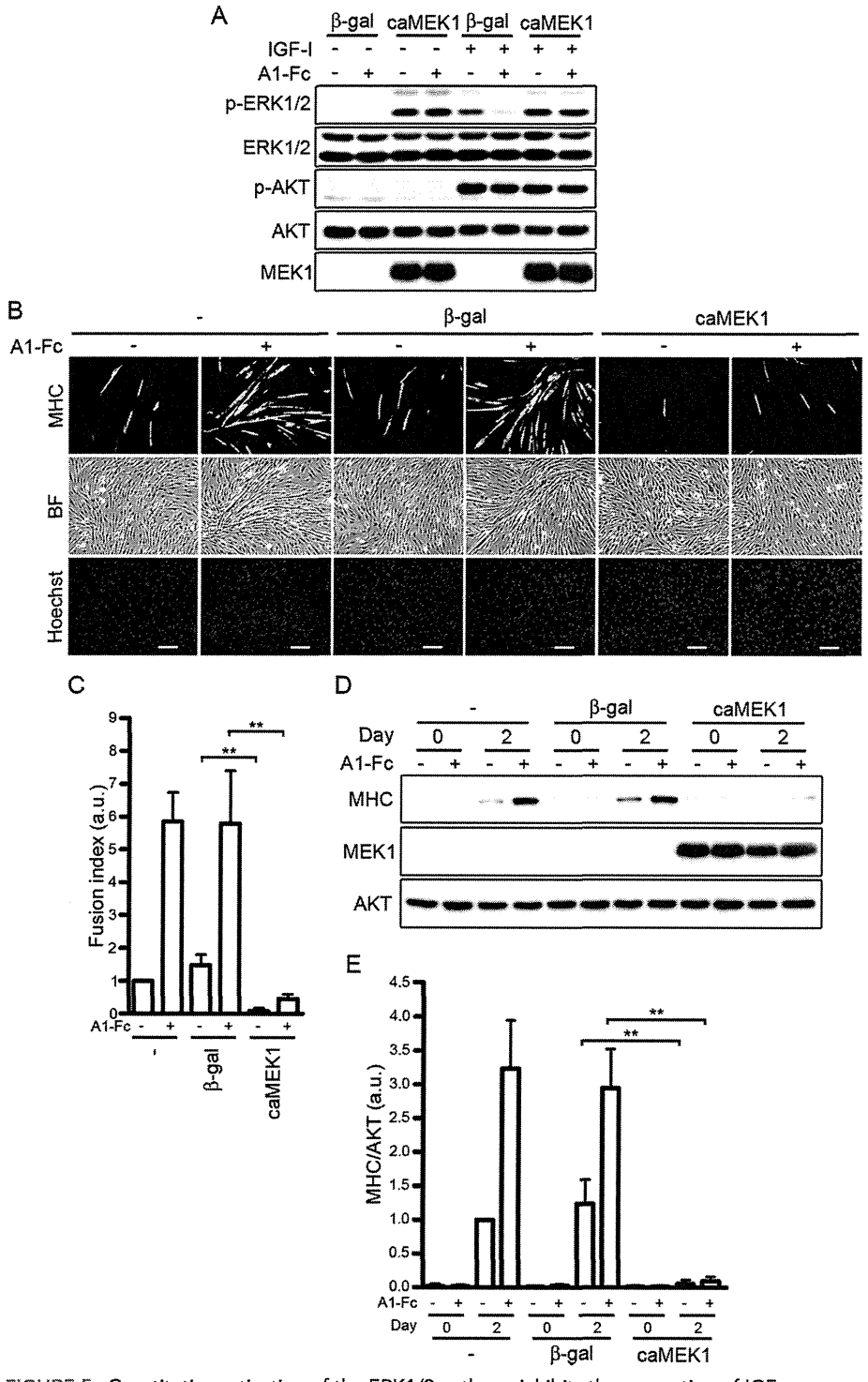

FIGURE 5: Constitutive activation of the ERK1/2 pathway inhibits the promotion of IGF-I–mediated myogenic differentiation by the ephrinA/EphA signal. (A) Serum-starved C2C12 myoblasts infected with adenoviruses encoding either β-gal (β-gal) or constitutive active mutant of MEK1 (caMEK1) were stimulated with or without 10 nM IGF-I for 10 min in the presence of 1.7 nM Fc (–) or ephrinA1-Fc (A1-Fc) as indicated at the top. Cell lysates were subjected to Western blot analysis with anti–phospho-ERK1/2 (p-ERK1/2), anti-ERK1/2 (ERK1/2), anti–phospho-AKT (p-AKT), anti-AKT (AKT), and MEK1 (MEK1) antibodies as indicated at the left. (B) C2C12 myoblasts infected without (–) or with adenoviruses encoding either β-gal (β-gal) or constitutive active mutant of MEK1 (caMEK1) were differentiated into myotubes in DMEM containing 1% FBS and 10 nM IGF-I in the presence of 6.4 nM Fc (–) or ephrinA1-Fc (A1-Fc) for 2 d. The cells were immunostained with anti-MHC antibody, and visualized with Alexa Fluor 488–conjugated secondary antibody. The cells were also poststained with Hoechst 33342 to visualize the nuclei. Alexa 488 (MHC), bright-field (BF), and Hoechst 33342 (Hoechst) images are shown as indicated at the left. Experiments were repeated three times with similar results. Scale bars, 100 μm. (C) The fusion index observed in B was determined as described in the legend of Figure 3B. Values are expressed relative to that observed in the uninfected cells differentiated in the presence of Fc and shown as means ± SD of three independent experiments. (D) Adenovirus-infected C2C12 myoblasts were differentiated into myotubes as described in B for time periods (days) indicated at the top. Cell lysates were subjected to Western blot analysis using anti-MHC (MHC), anti-MEK1 (MEK1), and anti-AKT (AKT) antibodies as indicated at the left. (E) The expression level of MHC observed in D was quantified by normalizing the expression of MHC by that of AKT. Values are expressed relative to that observed in the uninfected cells differentiated in the presence of Fc for 2 d and shown as means ± SD of three independent experiments. **$p < 0.01$, significant differences between two groups. a.u., arbitrary unit(s).

implicated in differentiation of primary myoblasts or in myogenic differentiation in vivo.

The present study apparently indicates that p120RasGAP-mediated inhibition of the Ras–ERK1/2 pathway is responsible for the promotion of myogenic differentiation by the ephrinA/EphA signal in myoblast cell lines. However, since the ephrinA/EphA signal not only activates p120RasGAP but also stimulates various intracellular signaling molecules (Pasquale, 2010), myogenic differentiation might also be regulated by other signaling pathways. EphA2 signaling is known to promote the intercellular junctions mediated by cadherins such as E-cadherin and N-cadherin (Miao *et al.*, 2003; Cooper *et al.*, 2008; Jun *et al.*, 2009; Miura *et al.*, 2009). Because engagement of N-cadherin and M-cadherin leads to the activation of promyogenic signaling pathways in myoblasts (Krauss, 2010), the ephrinA/EphA signal may promote skeletal myogenesis by enhancing cadherin-based cell–cell junctions. RhoA is activated by EphA receptors through ephexin (Shamah *et al.*, 2001) and induces expression of muscle-specific genes through serum response factor (Carnac *et al.*, 1998). Thus the ephrinA/EphA signal may also regulate myogenesis through RhoA-dependent expression of muscle-specific genes. In addition, it has been shown that ephrinA-mediated reverse signaling also regulates various biological functions, such as insulin secretion from β cells, neurogenesis, tumor suppression, and tumor progression (Pasquale, 2010). Thus it would be interesting to examine the involvement of ephrinA reverse signaling in myogenic differentiation.

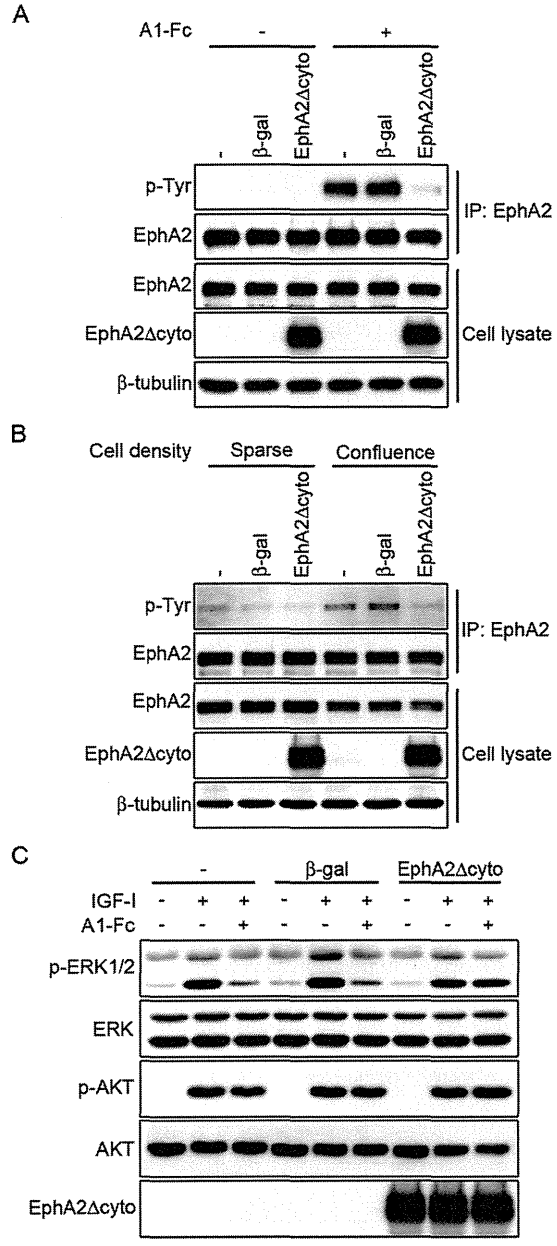

FIGURE 6: EphA2 mutant lacking the cytoplasmic region acts as a dominant-negative EphA receptor. (A) C2C12 myoblasts infected without (–) or with adenoviruses encoding either β-gal (β-gal) or C-terminal HA-tagged EphA2 mutant that lacks the cytoplasmic region (EphA2Δcyto) were serum starved and stimulated for 10 min in the presence of 2.2 nM Fc (–) or ephrinA1-Fc (A1-Fc) as indicated at the top. EphA2 was immunoprecipitated with anti-EphA2 antibody and subjected to Western blot analysis with anti-phosphotyrosine (p-Tyr) and anti-EphA2 (EphA2) antibodies. Aliquots of total-cell lysate were also subjected to Western blot analysis with anti-EphA2 (EphA2), anti-HA (EphA2Δcyto), and anti–β-tubulin (β-tubulin) antibodies as indicated at the left. (B) C2C12 myoblasts infected with adenoviruses as described in A were placed on the culture dishes for 4 h under either sparse or confluent culture condition as indicated at the top. Immunoprecipitation of EphA2 and Western blot analysis were performed as described in A. (C) C2C12 myoblasts infected with adenoviruses as described in A were serum starved and stimulated for 10 min with or without 10 nM IGF-I in the presence of 1.7 nM Fc (–) or ephrinA1-Fc (A1-Fc) as indicated at the top. Cell lysates were subjected to Western blot analysis with anti–phospho-ERK1/2 (p-ERK1/2), anti-ERK1/2 (ERK1/2), anti–phospho-AKT (p-AKT), anti-AKT (AKT), and anti-HA (EphA2Δcyto) antibodies as indicated at the left.

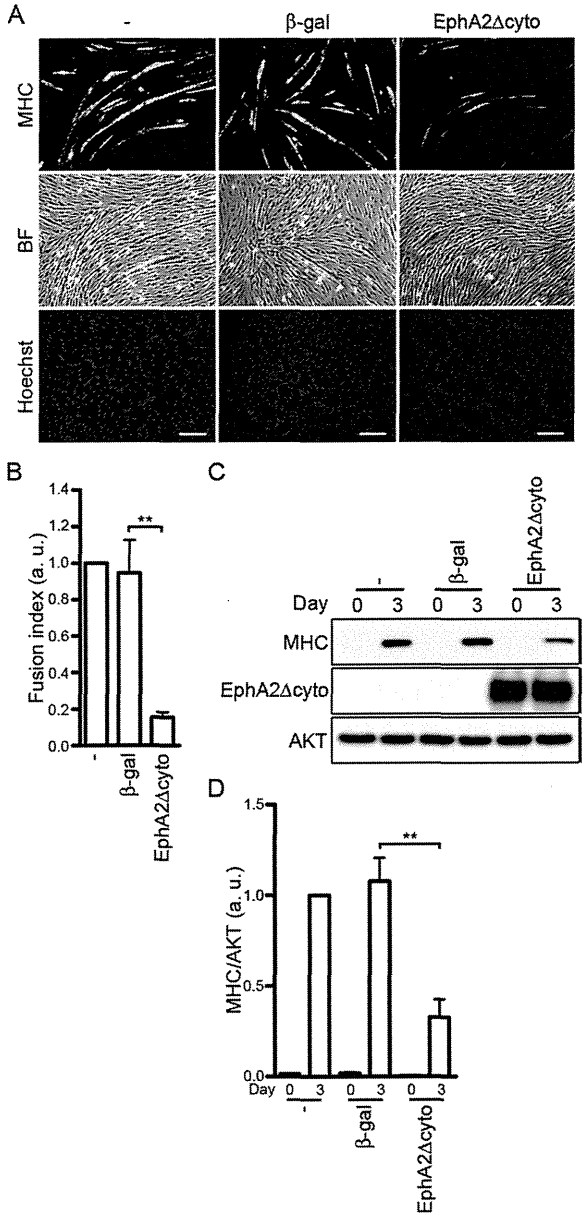

FIGURE 7: IGF-I–induced myogenic differentiation is blunted by blocking the ephrinA/EphA signal. (A) C2C12 myoblasts infected without (–) or with adenoviruses encoding either β-gal or EphA2Δcyto were differentiated into myotubes in DMEM containing 1% FBS and 10 nM IGF-I for 3 d. The cells were immunostained with anti-MHC antibody and visualized with Alexa Fluor 488–conjugated secondary antibody. The cells were also poststained with Hoechst 33342 to visualize the nuclei. Alexa 488 (MHC), bright-field (BF), and Hoechst 33342 (Hoechst) images are shown as indicated at the left. Experiments were repeated three times with similar results. Scale bars, 100 μm. (B) The fusion index observed in A was determined as described in the legend of Figure 3B. Values are expressed relative to that observed in the uninfected cells and shown as means ± SD of three independent experiments. (C) Adenovirus-infected C2C12 myoblasts were differentiated into myotubes as described in A for time periods (days) indicated at the top. Cell lysates were subjected to Western blot analysis using anti-MHC (MHC), anti-HA (EphA2Δcyto), and anti-AKT (AKT) antibodies as indicated at the left. (D) The expression level of MHC observed in C was quantified by normalizing the expression of MHC by that of AKT. Values are expressed relative to that observed in the uninfected cells differentiated for 3 d and shown as means ± SD of three independent experiments. **$p < 0.01$, significant differences between two groups. a.u., arbitrary unit(s).

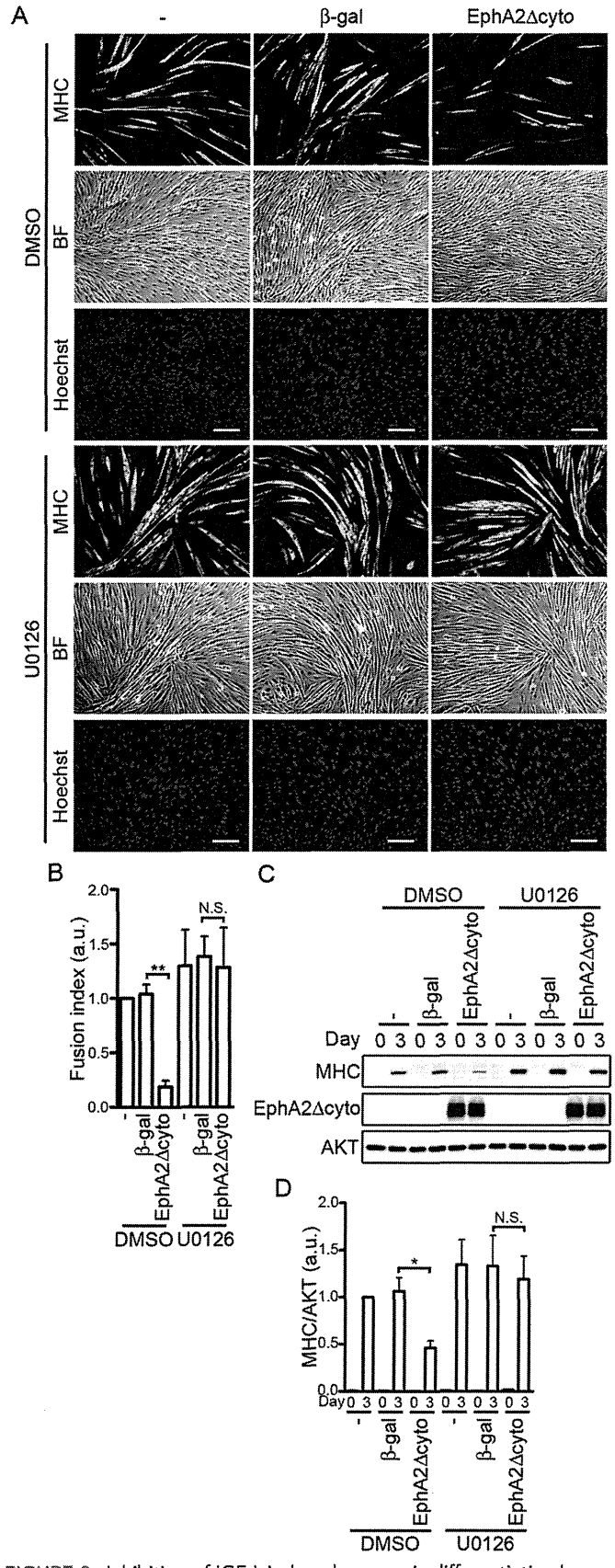

FIGURE 8: Inhibition of IGF-I–induced myogenic differentiation by a dominant-negative EphA receptor mutant is canceled by inhibiting the ERK1/2 pathway. (A) C2C12 myoblasts infected without (–) or with adenoviruses encoding either β-gal or EphA2Δcyto were differentiated into myotubes in DMEM containing 1% FBS and 10 nM IGF-I in the presence of vehicle (dimethyl sulfoxide [DMSO]) or 3 μM U0126 for 3 d. The cells were immunostained with anti-MHC antibody and visualized with Alexa Fluor 488–conjugated secondary antibody. The cells were also poststained with Hoechst 33342 to visualize the nuclei. Alexa 488 (MHC), bright-field (BF), and Hoechst 33342 (Hoechst) images are shown as indicated at the left. Experiments were repeated three times with similar results. Scale bars, 100 μm. (B) The fusion index observed in A was determined as described in the legend of Figure 3B. Values are expressed relative to that observed in the uninfected cells differentiated in the presence of DMSO and shown as means ± SD of three independent experiments. (C) Adenovirus-infected C2C12 myoblasts were differentiated into myotubes as described in A for time periods (days) indicated at the top. Cell lysates were subjected to Western blot analysis using anti-MHC (MHC), anti-HA (EphA2Δcyto), and anti-AKT (AKT) antibodies as indicated at the left. (D) The expression level of MHC observed in C was quantified by normalizing the expression of MHC by that of AKT. Values are expressed relative to that observed in the uninfected cells differentiated in the presence of DMSO for 3 d and shown as means ± SD of three independent experiments. *$p < 0.05$, **$p < 0.01$, significant differences between two groups. N.S., no significance between two groups. a.u., arbitrary unit(s).

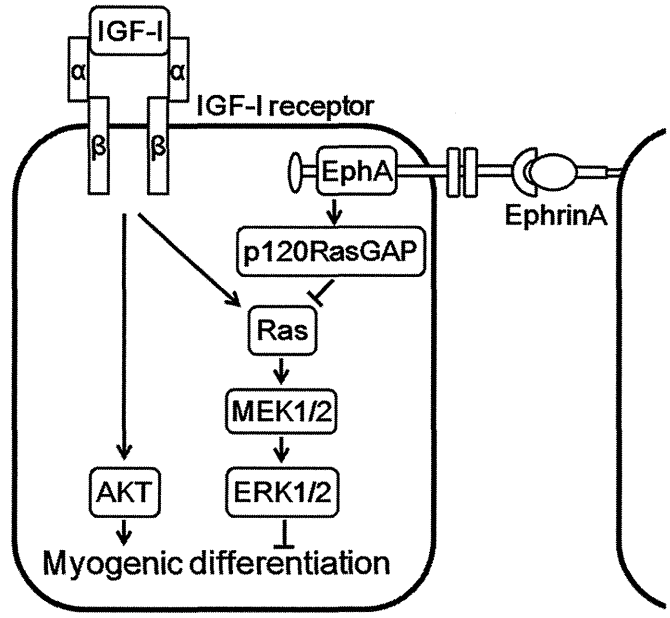

FIGURE 9: Schematic representation of a proposed model for how the ephrinA/EphA signal potentiates IGF-I–induced myogenic differentiation. IGF-I not only induces myogenic differentiation through the PI3K/AKT pathway but also stimulates the myogenic inhibitory signal mediated by the Ras–ERK1/2 cascade. The cell–cell contact–dependent ephrinA/EphA signal suppresses the RasxERK1/2 cascade by IGF-I through p120RasGAP, thereby facilitating IGF-I–mediated myogenic differentiation.

In conclusion, we have demonstrated that the cell–cell contact–dependent ephrinA/EphA signal suppresses IGF-I–induced activation of the Ras–ERK1/2 cascade by decreasing the Ras activity through p120RasGAP in myoblast cell lines. This molecular mechanism accounts for IGF-I–induced myogenic differentiation facilitated by ephrinA/EphA.

MATERIALS AND METHODS

Reagents and antibodies

COMP-Ang1 was kindly provided by G. Y. Koh (Korea Advanced Institute of Science and Technology, Daejeon, South Korea). Human

recombinant IGF-I was kindly provided by Astellas Pharma (Tokyo, Japan). Other reagents were purchased as follows: Hoechst 33342 nuclear dye from Sigma-Aldrich (St. Louis, MO); human Fc, mouse ephrinA1-Fc, and mouse ephrinB1-Fc from R&D Systems (Minneapolis, MN); and U0126 from Cell Signaling Technology (Beverly, MA). Antibodies were purchased as follows: anti–phospho-p44/42 ERK1/2 (Thr-202/Tyr-204), anti–phospho-AKT (Thr-308), and anti-AKT from Cell Signaling Technology; anti-MEK1, anti-ERK1/2, anti-EphA2, and anti-phosphotyrosine (PY99) from Santa Cruz Biotechnology (Santa Cruz, CA); anti-HA tag from Roche Diagnostics (Indianapolis, IN); anti–pan Ras from Calbiochem (La Jolla, CA); anti-MHC (MF20) from the Developmental Studies Hybridoma Bank (Iowa City, IA); anti–β-tubulin from Sigma-Aldrich; horseradish peroxidase–conjugated anti-mouse, anti-rabbit, and anti-rat from GE Healthcare Life Sciences (Piscataway, NJ); and Alexa Fluor 488–labeled goat anti–mouse IgG from Molecular Probes (Eugene, OR).

Cell culture, stimulation, and myogenic differentiation

Mouse C2C12 and rat L6 myoblasts were maintained as subconfluent monolayers in DMEM (Nissui, Tokyo, Japan) supplemented with FBS (20% for C2C12 cells, 10% for L6 cells), 4.5 g/l glucose, 0.58 g/l L-glutamine, 100 U/ml penicillin, and 100 μg/ml streptomycin. To examine the IGF-I–induced activation of ERK1/2, AKT, and Ras, the cells were serum starved overnight and stimulated with IGF-I in the presence or absence of nonclustered Fc, ephrinA1-Fc, or ephrinB1-Fc as indicated in the figure legends. For the induction of myogenic differentiation, cultured medium was replaced with DMEM containing 1% FBS and IGF-I at the concentrations described in the figure legends, when cell density reached confluency. The differentiation medium was exchanged every day. Human umbilical vein endothelial cells were purchased from Kurabo (Osaka, Japan) and maintained as described previously (Fukuhara *et al.*, 2005).

siRNA-mediated protein knockdown

Stealth siRNAs targeting mouse p120RasGAP (no. 1, 5′-UGUCCAACACCUAACAACCAGUUUA-3′; no. 2, 5′-CACUACUGGCCAGCAUCCUACUAAA-3′) and siRNA duplexes with irrelevant sequences (Stealth RNAi negative control) as a control were purchased from Invitrogen (Carlsbad, CA). For siRNA-mediated gene silencing, 10 nM siRNA duplexes were introduced into C2C12 myoblasts by reverse transfection using Lipofectamine RNAiMAX reagent (Invitrogen) according to the manufacturer's instruction. The cells were replated 24–30 h after the transfection and subjected to the experiments.

Adenovirus vector construction and infection

To generate adenovirus vector expressing the human EphA2 mutant that lacks the cytoplasmic region (EphA2Δcyto), a cDNA fragment encoding amino acids 1–574 of human EphA2 was amplified by PCR using an expression vector for human EphA2 (a gift from A. Sakakibara, Nagoya University, Nagoya, Japan) as a template and was subcloned into pCMV-HA vector (Fukuhara *et al.*, 2008). Then, a cDNA fragment encoding C-terminal HA-tagged EphA2Δcyto was excised and inserted into the pShuttle vector (Clontech, Mountain View, CA). The adenovirus was produced by using the Adeno-X system according to the manufacturer's protocol (Clontech). Recombinant adenovirus vectors encoding β-gal and caMEK1 were kindly provided by M. Matsuda (Kyoto University, Kyoto, Japan) and S. Kawashima (Kobe University, Kobe, Japan), respectively. For adenoviral infection, subconfluent C2C12 cells were infected with adenoviruses at the multiplicity of infection of 30 for 24 h and replated for the experiments.

Immunoprecipitation and Western blot analysis

Cells were washed with ice-cold phosphate-buffered saline (PBS), lysed in lysis buffer containing 50 mM Tris, pH 7.5, 150 mM NaCl, 1 mM sodium orthovanadate, 20 mM sodium fluoride, 1% Nonidet P-40, 0.1% SDS, 0.5% sodium deoxycholate, and 1× protease inhibitor cocktail (Roche Diagnostics), and centrifuged at 15,000 × *g* for 20 min at 4°C. The supernatant was used as precleared total-cell lysate. For the immunoprecipitation of EphA2, the cells were lysed in lysis buffer containing 20 mM Tris, pH 7.5, 150 mM NaCl, 3 mM EDTA, 1% Nonidet P-40, and 1× protease inhibitor cocktail. EphA2 was immunoprecipitated from the cleared lysates by incubation with anti-EphA2 antibody for 2 h at 4°C. Immunocomplexes were recovered with the aid of protein A–Sepharose beads (GE Healthcare Life Sciences). Aliquots of cell lysate and the immunoprecipitates were subjected to SDS–PAGE and Western blot analysis with the antibodies as indicated in the figure legends.

Immunocytochemistry

Cells plated on 3.5-cm collagen type I–coated plastic dishes (Iwaki Asahi Glass, Tokyo, Japan) were fixed with 2% formaldehyde in PBS for 15 min, permeabilized with 0.1% Triton X-100 for 5 min, and blocked with PBS containing 4% bovine serum albumin for 1 h. The cells were then stained with anti-MHC antibody for 1 h at room temperature. Protein reacting with the antibody was visualized with Alexa Fluor 488–conjugated secondary antibody. The nucleus was also poststained with Hoechst 33342 nuclear dye. Fluorescent images of Alexa Fluor 488 and Hoechst 33342 and phase-contrast images were recorded with an Olympus IX-81 inverted fluorescence microscope (Olympus Corporation, Tokyo, Japan) as described previously (Noda *et al.*, 2010).

Reverse transcription-PCR

Total RNA was prepared from C2C12 myoblasts using TRIzol reagent (Invitrogen), and reverse-transcribed by random hexamer primers using Superscript II (Invitrogen) according to the manufacturer's instruction. PCR was performed using the gene-specific primers listed in the Supplemental Table S1. Amplification of glyceraldehyde-3-phosphate dehydrogenase was also performed in parallel as a control.

Detection of GTP-bound form of Ras

Ras activation was assessed using a pull-down technique. Cells were lysed at 4°C in a pull-down lysis buffer containing 20 mM Tris, pH 7.5, 100 mM NaCl, 10 mM $MgCl_2$, 1% Triton X-100, 1 mM ethylene glycol tetraacetic acid, 1 mM dithiothreitol, 1 mM sodium orthovanadate, and 1× protease inhibitor cocktail. GTP-bound Ras was collected on the glutathione transferase-tagged Ras binding domain of Raf precoupled to glutathione-Sepharose beads. GTP-bound Ras and aliquots of total cell lysate were subjected to Western blot analysis with the antibodies as indicated in the figure legends.

Statistical analysis

The signal intensity of the band of Western blot analysis was calculated using Scion Image software. All data are expressed as means ± SD. Differences among multiple groups were compared by one-way analysis of variance followed by a post hoc comparison tested with the Bonferroni method. Values of $p < 0.05$ were considered significant.

ACKNOWLEDGMENTS

We are grateful to G. Y. Koh (Korea Advanced Institute of Science and Technology) for COMP-Ang1, to A. Sakakibara (Nagoya University) for an expression vector for human EphA2, and to M. Matsuda

(Kyoto University) and S. Kawashima (Kobe University) for the adenovirus encoding β-gal and caMEK1, respectively. We also thank K. Nakaoka (Osaka University, Osaka, Japan) and K. Miura for helpful discussion and M. Sone, K. Hiratomi, H. Yonekawa, and Y. Matsuura for technical assistance. This work was supported in part by grants from the Ministry of Education, Science, Sports and Culture of Japan (to S.F. and N.M.), the Ministry of Health, Labor, and Welfare of Japan (to N.M.), the Program for the Promotion of Fundamental Studies in Health Sciences of the National Institute of Biomedical Innovation (to S.F. and N.M.), the Naito Foundation (to S.F.), the Takeda Science Foundation (to S.F. and N.M.), the Sagawa Foundation for Promotion of Cancer Research (to S.F.), the Mochida Memorial Foundation for Medical and Pharmaceutical Research (to S.F.), the Kowa Life Science Foundation (to S.F.), the Kanae Foundation for the Promotion of Medical Science (to S.F.), the Novartis Foundation (Japan) for the Promotion of Science (to S.F.), the Senri Life Science Foundation (to S.F.), the Mitsubishi Foundation (to N.M.), the Japan Cardiovascular Research Foundation (to S.F.), and an AstraZeneca Research Grant (to N.M.).

REFERENCES

Andres V, Walsh K (1996). Myogenin expression, cell cycle withdrawal, and phenotypic differentiation are temporally separable events that precede cell fusion upon myogenesis. J Cell Biol 132, 657–666.

Bach LA, Salemi R, Leeding KS (1995). Roles of insulin-like growth factor (IGF) receptors and IGF-binding proteins in IGF-II-induced proliferation and differentiation of L6A1 rat myoblasts. Endocrinology 136, 5061–5069.

Bennett AM, Tonks NK (1997). Regulation of distinct stages of skeletal muscle differentiation by mitogen-activated protein kinases. Science 278, 1288–1291.

Carnac G, Primig M, Kitzmann M, Chafey P, Tuil D, Lamb N, Fernandez A (1998). RhoA GTPase and serum response factor control selectively the expression of MyoD without affecting Myf5 in mouse myoblasts. Mol Biol Cell 9, 1891–1902.

Charrasse S, Comunale F, Fortier M, Portales-Casamar E, Debant A, Gauthier-Rouviere C (2007). M-cadherin activates Rac1 GTPase through the Rho-GEF trio during myoblast fusion. Mol Biol Cell 18, 1734–1743.

Charrasse S, Meriane M, Comunale F, Blangy A, Gauthier-Rouviere C (2002). N-cadherin-dependent cell-cell contact regulates Rho GTPases and beta-catenin localization in mouse C2C12 myoblasts. J Cell Biol 158, 953–965.

Cheng N, Brantley D, Fang WB, Liu H, Fanslow W, Cerretti DP, Bussell KN, Reith A, Jackson D, Chen J (2003). Inhibition of VEGF-dependent multistage carcinogenesis by soluble EphA receptors. Neoplasia 5, 445–456.

Clemmons DR (2009). Role of IGF-I in skeletal muscle mass maintenance. Trends Endocrinol Metab 20, 349–356.

Coolican SA, Samuel DS, Ewton DZ, McWade FJ, Florini JR (1997). The mitogenic and myogenic actions of insulin-like growth factors utilize distinct signaling pathways. J Biol Chem 272, 6653–6662.

Cooper MA, Son AI, Komlos D, Sun Y, Kleiman NJ, Zhou R (2008). Loss of ephrin-A5 function disrupts lens fiber cell packing and leads to cataract. Proc Natl Acad Sci USA 105, 16620–16625.

de Alvaro C, Martinez N, Rojas JM, Lorenzo M (2005). Sprouty-2 overexpression in C2C12 cells confers myogenic differentiation properties in the presence of FGF2. Mol Biol Cell 16, 4454–4461.

Elowe S, Holland SJ, Kulkarni S, Pawson T (2001). Downregulation of the Ras-mitogen-activated protein kinase pathway by the EphB2 receptor tyrosine kinase is required for ephrin-induced neurite retraction. Mol Cell Biol 21, 7429–7441.

Ewton DZ, Roof SL, Magri KA, McWade FJ, Florini JR (1994). IGF-II is more active than IGF-I in stimulating L6A1 myogenesis: greater mitogenic actions of IGF-I delay differentiation. J Cell Physiol 161, 277–284.

Florini JR, Ewton DZ, Coolican SA (1996). Growth hormone and the insulin-like growth factor system in myogenesis. Endocr Rev 17, 481–517.

Florini JR, Magri KA, Ewton DZ, James PL, Grindstaff K, Rotwein PS (1991). "Spontaneous" differentiation of skeletal myoblasts is dependent upon autocrine secretion of insulin-like growth factor-II. J Biol Chem 266, 15917–15923.

Fukuhara S, Sako K, Minami T, Noda K, Kim HZ, Kodama T, Shibuya M, Takakura N, Koh GY, Mochizuki N (2008). Differential function of Tie2 at cell-cell contacts and cell-substratum contacts regulated by angiopoietin-1. Nat Cell Biol 10, 513–526.

Fukuhara S, Sakurai A, Sano H, Yamagishi A, Somekawa S, Takakura N, Saito Y, Kangawa K, Mochizuki N (2005). Cyclic AMP potentiates vascular endothelial cadherin-mediated cell-cell contact to enhance endothelial barrier function through an Epac-Rap1 signaling pathway. Mol Cell Biol 25, 136–146.

Gavard J, Marthiens V, Monnet C, Lambert M, Mege RM (2004). N-cadherin activation substitutes for the cell contact control in cell cycle arrest and myogenic differentiation: involvement of p120 and beta-catenin. J Biol Chem 279, 36795–36802.

Guasconi V, Puri PL (2009). Chromatin: the interface between extrinsic cues and the epigenetic regulation of muscle regeneration. Trends Cell Biol 19, 286–294.

Gutierrez J, Brandan E (2010). A novel mechanism of sequestering fibroblast growth factor 2 by glypican in lipid rafts, allowing skeletal muscle differentiation. Mol Cell Biol 30, 1634–1649.

Jun G *et al.* (2009). EPHA2 is associated with age-related cortical cataract in mice and humans. PLoSGenet 5, e1000584.

Kaliman P, Canicio J, Shepherd PR, Beeton CA, Testar X, Palacin M, Zorzano A (1998). Insulin-like growth factors require phosphatidylinositol 3-kinase to signal myogenesis: dominant negative p85 expression blocks differentiation of L6E9 muscle cells. Mol Endocrinol 12, 66–77.

Kaliman P, Vinals F, Testar X, Palacin M, Zorzano A (1996). Phosphatidylinositol 3-kinase inhibitors block differentiation of skeletal muscle cells. J Biol Chem 271, 19146–19151.

Kang JS, Bae GU, Yi MJ, Yang YJ, Oh JE, Takaesu G, Zhou YT, Low BC, Krauss RS (2008). A Cdo-Bnip-2-Cdc42 signaling pathway regulates p38alpha/beta MAPK activity and myogenic differentiation. J Cell Biol 182, 497–507.

Kang JS, Yi MJ, Zhang W, Feinleib JL, Cole F, Krauss RS (2004). Netrins and neogenin promote myotube formation. J Cell Biol 167, 493–504.

Kim I, Ryu YS, Kwak HJ, Ahn SY, Oh JL, Yancopoulos GD, Gale NW, Koh GY (2002). EphB ligand, ephrinB2, suppresses the VEGF- and angiopoietin-1-induced Ras/mitogen-activated protein kinase in venous endothelial cells. FASEB J 16, 1126–1128.

Koyama T *et al.* (2008). Interaction of scaffolding adaptor protein Gab1 with tyrosine phosphatase SHP2 negatively regulates IGF-I-dependent myogenic differentiation via the ERK1/2 signaling pathway. J Biol Chem 283, 24234–24244.

Krauss RS (2010). Regulation of promyogenic signal transduction by cell-cell contact and adhesion. Exp Cell Res 316, 3042–3049.

Lai KO, Chen Y, Po HM, Lok KC, Gong K, Ip NY (2004). Identification of the Jak/Stat proteins as novel downstream targets of EphA4 signaling in muscle: implications in the regulation of acetylcholinesterase expression. J Biol Chem 279, 13383–13392.

Liu JP, Baker J, Perkins AS, Robertson EJ, Efstratiadis A (1993). Mice carrying null mutations of the genes encoding insulin-like growth factor I (Igf-1) and type 1 IGF receptor (Igf1r). Cell 75, 59–72.

Lovett FA, Gonzalez I, Salih DA, Cobb LJ, Tripathi G, Cosgrove RA, Murrell A, Kilshaw PJ, Pell JM (2006). Convergence of Igf2 expression and adhesion signalling via RhoA and p38 MAPK enhances myogenic differentiation. J Cell Sci 119, 4828–4840.

Lu M, Krauss RS (2010). N-cadherin ligation, but not Sonic hedgehog binding, initiates Cdo-dependent p38alpha/beta MAPK signaling in skeletal myoblasts. Proc Natl Acad Sci USA 107, 4212–4217.

Macrae M, Neve RM, Rodriguez-Viciana P, Haqq C, Yeh J, Chen C, Gray JW, McCormick F (2005). A conditional feedback loop regulates Ras activity through EphA2. Cancer Cell 8, 111–118.

Miao H, Nickel CH, Cantley LG, Bruggeman LA, Bennardo LN, Wang B (2003). EphA kinase activation regulates HGF-induced epithelial branching morphogenesis. J Cell Biol 162, 1281–1292.

Miao H, Wei BR, Peehl DM, Li Q, Alexandrou T, Schelling JR, Rhim JS, Sedor JR, Burnett E, Wang B (2001). Activation of EphA receptor tyrosine kinase inhibits the Ras/MAPK pathway. Nat Cell Biol 3, 527–530.

Miura K, Nam JM, Kojima C, Mochizuki N, Sabe H (2009). EphA2 engages Git1 to suppress Arf6 activity modulating epithelial cell-cell contacts. Mol Biol Cell 20, 1949–1959.

Noda K, Zhang J, Fukuhara S, Kunimoto S, Yoshimura M, Mochizuki N (2010). Vascular endothelial-cadherin stabilizes at cell-cell junctions by anchoring to circumferential actin bundles through α- and β-catenins in cyclic AMP-Epac-Rap1 signal-activated endothelial cells. Mol Biol Cell 21, 584–596.

Parri M, Buricchi F, Taddei ML, Giannoni E, Raugei G, Ramponi G, Chiarugi P (2005). EphrinA1 repulsive response is regulated by an EphA2 tyrosine phosphatase. J Biol Chem 280, 34008–34018.

Pasquale EB (2005). Eph receptor signalling casts a wide net on cell behaviour. Nat Rev Mol Cell Biol 6, 462–475.
Pasquale EB (2008). Eph-ephrin bidirectional signaling in physiology and disease. Cell 133, 38–52.
Pasquale EB (2010). Eph receptors and ephrins in cancer: bidirectional signalling and beyond. Nat Rev Cancer 10, 165–180.
Pavlath GK (2010). Spatial and functional restriction of regulatory molecules during mammalian myoblast fusion. Exp Cell Res 316, 3067–3072.
Shamah SM *et al.* (2001). EphA receptors regulate growth cone dynamics through the novel guanine nucleotide exchange factor ephexin. Cell 105, 233–244.
Swartz ME, Eberhart J, Pasquale EB, Krull CE (2001). EphA4/ephrin-A5 interactions in muscle precursor cell migration in the avian forelimb. Development 128, 4669–4680.
Taddei ML *et al.* (2009). Kinase-dependent and -independent roles of EphA2 in the regulation of prostate cancer invasion and metastasis. Am J Pathol 174, 1492–1503.
Takaesu G, Kang JS, Bae GU, Yi MJ, Lee CM, Reddy EP, Krauss RS (2006). Activation of p38alpha/beta MAPK in myogenesis via binding of the scaffold protein JLP to the cell surface protein Cdo. J Cell Biol 175, 383–388.
Taylor MV (2002). Muscle differentiation: how two cells become one. Curr Biol 12, R224–R228.
Tong J, Elowe S, Nash P, Pawson T (2003). Manipulation of EphB2 regulatory motifs and SH2 binding sites switches MAPK signaling and biological activity. J Biol Chem 278, 6111–6119.
Tortorella LL, Milasincic DJ, Pilch PF (2001). Critical proliferation-independent window for basic fibroblast growth factor repression of myogenesis via the p42/p44 MAPK signaling pathway. J Biol Chem 276, 13709–13717.
White MF (2003). Insulin signaling in health and disease. Science 302, 1710–1711.
Yokoyama T, Takano K, Yoshida A, Katada F, Sun P, Takenawa T, Andoh T, Endo T (2007). DA-Raf1, a competent intrinsic dominant-negative antagonist of the Ras-ERK pathway, is required for myogenic differentiation. J Cell Biol 177, 781–793.

ELSEVIER

A Potent Anti-angiogenic Factor, Vasohibin-1, Ameliorates Experimental Bronchiolitis Obliterans

T. Watanabe, Y. Okada, Y. Hoshikawa, S. Eba, H. Notsuda, Y. Watanabe, H. Ohishi, Y. Sato, and T. Kondo

ABSTRACT

Background. Bronchiolitis obliterans (BO) is a major cause of morbidity and mortality after lung transplantation. BO is pathologically characterized by neovascularized fibro-obliteration of the allograft airway. A recent study has shown that aberrant angiogenesis during fibro-obliteration contributes to the pathogenesis of BO. Vasohibin-1 (VASH1) has been isolated as a vascular endothelial growth factor–inducible gene in endothelial cells (ECs) that inhibits migration and proliferation of ECs and exhibits anti-angiogenic activity in vivo.

Purpose. This study examines whether VASH1 inhibits fibro-obliteration of the allograft in a murine intrapulmonary tracheal transplantation model.

Method. Tracheal allografts of BALB/c mouse were transplanted into the left lung of recipient C57BL/6J mouse. We performed gene transfer to the recipient lungs using an adenovirus vector encoding human VASH1 (Ad-VASH1) or beta- garactosidase (Ad-LacZ) as the control. Tracheal allografts were harvested and pathological on days 21 and 28.

Result. Ad-VASH1 treatment reduced the vascular area on day 21 (4.6% versus 13.0%, $P = .037$) and day 28 (5.4% versus 13.4%, $P = .022$) compared with the control group. This was accompanied by significantly inhibited luminal obliteration of the tracheal allografts in the animals transferred with Ad-VASH1 compared with the control (69% versus 93%, $P = .028$) on day 21. We were not able to observe this effect on day 28 (92% versus 97%, $P = .48$).

Conclusion. Transgene expression of VASH1 in the recipient lung significantly attenuated luminal obliteration of the tracheal allograft; this was associated with significantly reduced aberrant angiogenesis in the fibro-obliterative tissue in a murine model intrapulmonary tracheal transplantation.

BRONCHIOLITIS obliterans (BO) is a major obstacle to the long-term survival of lung transplant recipients. The clinical manifestation of BO, bronchiolitis obliterans syndrome (BOS), develops in 50% of all lung transplant recipients and accounts for 30% of recipient death at 5 years after transplantation.[1] Although the mechanisms involved in the etiology of BO are not fully understood, it is generally accepted that it develops as a result of persistent immunological and inflammatory insults to the allograft airways that cause epithelial injury, granulation tissue formation, and, ultimately, fibro-obliteration of the airways.

Angiogenesis is the formation of new blood vessels; it plays a central role in the progression of various chronic inflammatory diseases including diabetic retinopathy, rheu-

From the Department of Thoracic Surgery (T.W., Y.O., Y.H., S.E., H.N., H.O., T.K.), and the Department of Vascular biology (T.W., Y.S.), Institute of Development, Aging and Cancer, Tohoku University, Sendai, Japan.

Address reprint requests to Yoshinori Okada, Department of Thoracic Surgery, Institute of Development, Aging and Cancer, Tohoku University, 4-1 Seiryo-machi, Aoba-ku, Sendai, Miyagi, Japan, 980-8575. E-mail: yokada@idac.tohoku.ac.jp

0041-1345/–see front matter
doi:10.1016/j.transproceed.2012.02.022

matoid arthritis, and pulmonary fibrosis.[2] These diseases are characterized by chronic inflammation and fibroproliferation associated with marked vascular remodeling. Although a number of studies have focused on angiogenesis in the development of these chronic inflammatory diseases, little attention has been paid to the role of angiogenesis in the process of BO. Recently, Belperio et al showed that the CXC chemokine receptor 2/CXC chemokine receptor 2 ligand biological axis is responsible for aberrant angiogenesis and supports the fibroproliferative process in human BOS and in a murine model of BO.[3] This study proposes a novel therapeutic strategy designed to attenuate vascular remodeling to prevent BO after lung transplantation. No other studies focusing on modulation of vascular remodeling, however, have been reported in preventing or treating BO.

Vasohibin-1 (VASH1) has been isolated as a vascular endothelial growth factor–inducible gene from endothelial cells (ECs). VASH1 inhibits migration and proliferation of ECs in culture and exhibits a potent anti-angiogenic activity in vivo.[4,5] We hypothesized that VASH1 may inhibit aberrant angiogenesis that supports the process of fibroproliferation observed in BO. The purpose of the present study is to examine whether VASH1 inhibits fibro-obliteration of the tracheal allografts in an experimental murine model of BO.

MATERIALS AND METHOD

Animals

Pathogen-free, 6- to 7-weeks-old male BALB/c (H2-d) and C57BL/6 (H-2b) mice were commercially obtained from Charles River Laboratories Japan, Inc (Yokohama, Japan) and housed and used in accordance with the rules of the Institutional Animal Care and Use Committee.

Adenovirus Vectors

A replication-defective adenovirus vector encoding human VASH1 gene (Ad-VASH1) and beta-galactosidase gene (Ad-LacZ) used as the control were prepared as previously described.[6] Briefly, plaque-purified adenoviruses were propagated in HEK293 cells. The viral lysates were purified and concentrated through two cycles of cesium chloride step gradients.

Experimental Design

Intrapulmonary tracheal transplantation was performed as previously described.[7] BALB/c tracheas were transplanted into the left lung parenchyma of the C57BL/6J mice. Ad-VASH1 or Ad-LacZ adjusted to 1.0×10^9 plaque forming units per 75 μL was intratracheally administered to the recipient mice on days 6, 13, and 20 posttransplantation. Our preliminary studies using a reporter gene showed the feasible gene transfer to the both lungs with this procedure. Human VASH1 messenger RNA was readily detectable in the recipient left lung transferred with Ad-VASH1 and harvested on day 21 posttransplantation and not in the lung transferred with Ad-LacZ (data not shown). Mice were sacrificed and the left lungs bearing allografts harvested on days 21 (n = 10, 8) and 28 (n = 5, 4) posttransplantation.

Histology and Immunohistochemistry

The removed lungs were immediately fixed in 4% parafolmaldehyde. After 24 hours of fixation, they were embedded in paraffin, sectioned, and stained with hematoxylin and eosin. To examine the intensity of angiogenesis, immunohistochemical staining for CD31 was performed. Sections were deparaffinized and incubated for 5 minutes at 120°C. Primary antibody reactions were performed using an anti-CD31 antibody (Santa Cruz Biotechnology, Santa Cruz, Calif, United States) with a dilution of 1:600 overnight at 4°C. Antibody depositions were visualized using diaminobenzidine. Nuclei were counterstained with hematoxylin.

Measurement of Luminal Obliteration and Vascular Area of the Tracheal Allografts

Histological sections of the allografts were photographed at an original magnification of × 10 with an all-in-one microscope with a computer (BZ9000, Keyence, Tokyo, Japan). The percentage of luminal obliteration in the tracheal allografts was calculated using the analysis software provided by Keyence as previously described.[8] Vascular area as shown by the sum total of the lumina surrounded by CD31-positive ECs in the fibroproliferative tissue was also calculated as previously described.[9] Vascular area was normalized by area of fibro-obliteration.

Statistical Analyses

Data were expressed as the mean ± SE. The significance of the difference between the groups was determined by Student *t* test. All statistical analyses were performed using GraphPad PRISM (GraphPad Software Inc, San Diego, Calif, United States). Values of $P \leqq .05$ were considered to be significant.

RESULTS

Effect of Ad-VASH1 Gene Transfer on Luminal Obliteration and Vascular Area of the Tracheal Allografts

On day 21 posttransplantation, the lumen of the tracheal allografts in the lung expressing LacZ was almost completely obstructed, whereas the lumen of the most of allografts in the lung expressing VASH1 was partially opened. Luminal obliteration of the tracheal allograft was significantly attenuated in the animals transferred with Ad-VASH1 compared with the controls transferred with Ad-LacZ (69% versus 93%, $P = .0276$; Fig 1). Vascular area in the fibroproliferative tissue was also significantly reduced in allografts in the animals transferred with Ad-VASH1 compared with those with Ad-LacZ (4.6% versus 13.0%, $P = .037$; Fig 2).

On day 28 posttransplantation, luminal obliteration of the tracheal allograft was almost similar in the both groups with no statistically significant difference between the groups (92% versus 97%, $P = .48$). Vascular area in the fibroproliferative tissue was still significantly reduced in the allografts in the animals transferred with Ad-VASH1 compared with those with Ad-LacZ (5.4% versus 13.4%, $P = .022$).

DISCUSSION

A novel model for posttransplantation obliterative airway disease in which the trachea is transplanted into the lung

parenchyma was introduced by Andre et al in 2005.[10] In this model, the blood supply to the tracheal graft derives from the pulmonary circulation. This model is valuable for studying the mechanisms of fibrous obliteration of the transplanted airway in the relevant local environment of the lung and also makes it possible to study pulmonary-targeted therapies with transvascular and trans-airway routes.

The present study showed that transgene expression of VASH1 in the recipient lung significantly attenuated luminal obliteration of the tracheal allograft and this was associated with significantly reduced aberrant angiogenesis in the fibro-obliterative tissue when allografts were examined on day 21 posttransplantation. This finding primarily supports the hypothesis that vascular remodeling due to aberrant angiogenesis during fibro-obliteration of the allograft airway contributes at least in part to the pathogenesis of fibro-obliterative airway disease, as seen in other chronic inflammatory diseases. The vascular remodeling of the tracheal allograft was also inhibited by VASH1 when the allograft was harvested on day 28 posttransplantation, whereas luminal obliteration was not significantly ameliorated. This may be due to the nature of transient transgene expression of target protein with this gene delivery system that may not express sufficient amount of the target protein in the late phase after gene transfer. Another possibility is that the result reflects the limitation of the effect of anti-angiogenic approaches in preventing BO. Further studies are desirable to more clearly understand the role of angiogenesis in the pathogenesis of BO and also the effect of antiangiongenic therapy on preventing BO.

In conclusion, transgene expression of a potent anti-angiogenic substance (VASH1), in the recipient lung significantly attenuated luminal obliteration of the tracheal allograft and this was associated with significantly reduced aberrant angiogenesis in the fibro-obliterative tissue in a murine model of intrapulmonary tracheal transplantation. Therapeutic potential of anti-angiogenic agents targeting BO merits further investigations.

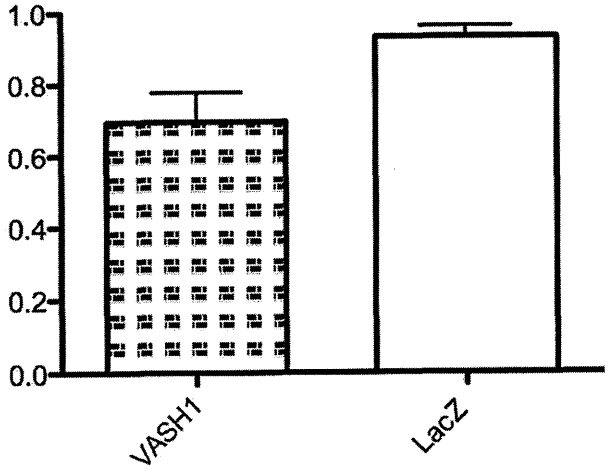

Fig 1. Luminal obliteration was significantly attenuated by VASH1 in the allografts harvested on day21 post-transplant (93% versus 69%, $P = .0276$).

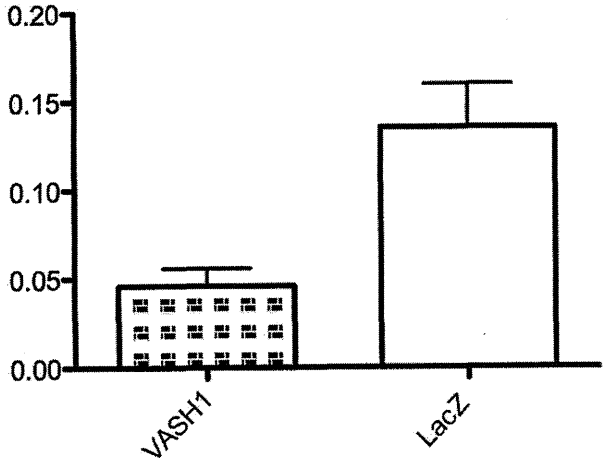

Fig 2. Vash1 treatment reduced vascular area in the allografts on day 21 posttransplant (13.0% versus 4.6%, $P = .037$).

REFERENCES

1. Christie JD, Edwards LB, Aurora P, et al: Registry of the International Society for Heart and Lung Transplantation: twenty-fifth official adult lung and heart/lung transplantation report—2008. J Heart Lung Transplant 27:957, 2008

2. Sivakumar B, Harry LE, Paleolog EM: Modulating angiogenesis: more vs. less. JAMA 292:972, 2004

3. Belperio JA, Keane MP, Burdick MD, et al: Role of CXCR2/CXCR2 ligands in vascular remodeling during bronchiolitis obliterans syndrome. J Clin Invest 115:1150, 2005

4. Watanabe K, Hasegawa Y, Yamashita H, et al: Vasohibin as an endothelium-derived negative feedback regulator of angiogenesis. J Clin Invest 114:898, 2004

5. Heishi T, Hosaka T, Suzuki Y, et al: Endogenous angiogenesis inhibitor vasohibin1 exhibits broad-spectrum antilymphangiogenic activity and suppresses lymph node metastasis. Am J Pathol 176:1950, 2010

6. Hosaka T, Kimura H, Heishi T, et al: Vasohibin-1 expression in endothelium of tumor blood vessels regulates angiogenesis. Am J Pathol 175:430, 2009

7. Hirayama S, Sato M, Liu M, et al: Local long-term expression of lentivirally delivered IL-10 in the lung attenuates obliteration of intrapulmonary allograft airways. Hum Gene Ther 22:1453, 2011

8. Lau CL, Zhao Y, Kron IL, et al: The role of adenosine A2A receptor signaling in bronchiolitis obliterans. Ann Thorac Surg 88:1071, 2009

9. Kimura H, Miyashita H, Suzuki Y, et al: Distinctive localization and opposed roles of vasohibin-1 and vasohibin-2 in the regulation of angiogenesis. Blood 113:4810, 2009

10. Dutly AE, Andrade CF, Verkaik R, et al: A novel model for post-transplant obliterative airway disease reveals angiogenesis from the pulmonary circulation. Am J Transplant 5:248, 2005

Published OnlineFirst June 6, 2012; DOI: 10.1158/1078-0432.CCR-12-0073

Clinical Cancer Research

Imaging, Diagnosis, Prognosis

The Prognostic Significance of Vasohibin-1 Expression in Patients with Upper Urinary Tract Urothelial Carcinoma

Yasumasa Miyazaki[1], Takeo Kosaka[1], Shuji Mikami[2], Eiji Kikuchi[1], Nobuyuki Tanaka[1], Takahiro Maeda[1], Masaru Ishida[1], Akira Miyajima[1], Ken Nakagawa[1], Yasunori Okada[2], Yasufumi Sato[3], and Mototsugu Oya[1]

Abstract

Purpose: Vasohibin-1 (VASH1) is a novel angiogenic molecule that is specifically expressed in activated vascular endothelial cells, and the status of VASH1 expression has been documented in cancer angiogenesis. The aim of this study was to address the prognostic value of VASH1 expression in upper urinary tract urothelial carcinomas (UTUC).

Experimental Design: We retrospectively analyzed the clinical records of 171 patients with locally advanced UTUC (Ta-3N0M0). The median follow-up period was 3.8 years. We immunohistochemically examined the accomplished microvessels with anti-CD34 as microvessel density (MVD) and the microvessels with activated endothelial cells as VASH1 density. Then, we analyzed the association between immunohistochemical expression and clinical outcomes.

Results: Forty-two patients experienced tumor recurrence and of these 34 died of the disease during follow-up. VASH1 density was significantly associated with tumor grade, pathologic T stage, and MVD. The 5-year recurrence-free and cancer-specific survival rates were 66.1% and 72.8% in patients with VASH1 density ($\geq 40/mm^2$) and 81.0% and 86.5% in their counterparts, respectively ($P < 0.05$). MVD was not an independent predictor of tumor recurrence or cancer-specific survival. Multivariate analyses revealed that high VASH1 density was an independent prognostic indicator of both tumor recurrence ($P = 0.024$, HR = 2.10) and cancer-specific survival ($P = 0.031$, HR = 2.23) as well as other standard prognostic factors including high tumor grade and lymphovascular invasion.

Conclusions: VASH1 density represents a clinically relevant predictor of patient prognosis in UTUC. The results suggest that VASH1 density could become a new biomarker and provide additional prognostic information in patients with UTUC. *Clin Cancer Res; 18(15); 4145–53. ©2012 AACR.*

Introduction

Upper urinary tract urothelial carcinoma (UTUC) is relatively rare, accounting for only 2% to 8% of all urothelial cancers (1). Although radical ipsilateral nephroureterectomy with excision of the bladder cuff remains the standard treatment in patients with localized UTUC, their prognosis is still poor due to local recurrence and distant metastasis following curative surgery (2). Many investigators have previously reported the possible predictors of tumor progression including local or distant recurrences of UTUC (3–6). The clinicopathologic parameters of UTUC, such as tumor stage, histologic grade, and lymphovascular invasion (LVI), have been reported to be independent predictors of clinical outcome following radical surgery (7). In addition to these standard predictors, several investigators evaluated relevant variables associated with tumor angiogenesis (8, 9). However, whether tumor angiogenesis could be a great predictor of UTUC outcome has not been fully evaluated yet.

Angiogenesis, that is the formation of new blood vessel networks, not only plays a role in human normal development, but also in pathophysiologic conditions such as inflammation and neoplasm. Angiogenic activity has been shown to clinically correlate with a greater incidence of metastasis and a poor prognosis for patients with neoplasm (10, 11). Angiogenesis is generally regulated by the balance between stimulatory and inhibitory factors. Angiogenic molecules such as CD34, von Willebrand factor, and vascular endothelial-cadherin, which are specifically expressed in vascular endothelial cells, could serve as biomarkers (12). However, those molecules are expressed in quiescent endothelial cells as well as in activated endothelial cells, and thus cannot fully reflect angiogenesis activity. One of the factors that provide information on angiogenesis activity in

Authors' Affiliations: Departments of [1]Urology and [2]Pathology, Keio University School of Medicine, Tokyo; and [3]Department of Vascular Biology, Institute of Development, Aging, and Cancer, Tohoku University, Sendai, Japan

Note Y. Miyazaki and T. Kosaka contributed equally to the work.

Corresponding Author: Mototsugu Oya, Department of Urology, Keio University School of Medicine, 35 Shinanomachi, Shinjuku-ku, Tokyo 1608582, Japan. Phone: 81-3-5363-3824; Fax: 81-3-3225-1985; E-mail: moto-oya@sc.itc.keio.ac.jp

doi: 10.1158/1078-0432.CCR-12-0073

Published OnlineFirst June 6, 2012; DOI: 10.1158/1078-0432.CCR-12-0073

Translational Relevance

Angiogenesis is intimately involved in tumor growth and distant metastasis. Although several parameters evaluating tumor angiogenesis such as the microvessel density (MVD) have been investigated, it has not been fully characterized yet that the MVD reflects the activity of tumor angiogenesis or the predictor of cancer progression. Recently, we isolated a novel angiogenic molecule, vasohibin-1 (VASH1), which is an intrinsic factor specifically expressed in activated vascular endothelial cells. Previous studies found that the expression of VASH1 was restricted to endothelial cells of blood vessels in the tumor stroma. In this study, we evaluated the VASH1 expression of tumor microvessels in upper urinary tract urothelial carcinoma (UTUC) and revealed that VASH1 definitely becomes a clinically relevant prognostic indicator. This report suggests that VASH1 could become a new molecular biomarker and provide additional prognostic information in patients with UTUC.

neoplasms or specific prognostic information, including urothelial carcinoma, is microvessel density (MVD). Several studies of urothelial carcinomas have indicated that MVD could be an independent negative prognostic factor (13–16). However, to date evidence of the prognostic role of MVD in urothelial carcinoma is contradictory (17–19).

We recently isolated a novel angiogenenic molecule, vasohibin-1 (VASH1), which is specifically expressed in endothelial cells and upregulated by VEGF and fibroblast growth factor-2 (FGF-2; refs. 20, 21). Previous studies found that the expression of VASH1 was restricted to endothelial cells of blood vessels in the tumor stroma and correlated with the expression of VEGF, FGF-2 in tumor cells (22). No one has ever characterized the expression of VASH1 in relation to tumor angiogenesis in UTUC. Therefore, we evaluated whether the expression of VASH1 could serve as a biomarker of tumor angiogenesis more accurately than MVD.

In the present study, we examined the expression of VASH1 and MVD in UTUC specimens acquired by primary surgery and retrospectively investigated whether VASH1 expression was related to tumor angiogenesis and clinical outcome in UTUC.

Materials and Methods

Patient selection

After obtaining Institutional Review Board approval, the medical records of patients operated on between 1983 and 2007 and archived at Keio University Hospital (Shinjuku-ku, Tokyo, Japan), were retrospectively reviewed. During this period, more than 200 patients underwent nephroureterectomy for UTUC at Keio University Hospital. Five patients with distant metastasis at diagnosis, 8 with pT4 and/or positive lymph node involvement, and 4 with concomitant muscle invasive bladder cancer were excluded from the analysis. After excluding 27 patients lost to follow-up within 6 months after surgery, we identified a total of 172 patients with locally advanced UTUC (pTa-3N0M0) in our study population. One patient who began to receive neoadjuvant chemotherapy before nephroureterectomy was excluded; thus, 171 patients were included in the subsequent analyses. The median follow-up of the whole cohort was 3.8 years (0.7–20). One hundred and forty-three patients (83.6%) had undergone open nephroureterectomy and 28 patients laparoscopic nephroureterectomy. Regional lymph nodes were dissected in patients with enlarged nodes on a preoperative evaluation or who were suspected of having enlarged nodes at intraoperative inspection. Extended lymphadenectomy was not routinely conducted. Cisplatin-based adjuvant chemotherapy regimens were administered to 28 patients (16.4%). Patients with pT3 tumors and presence of LVI were generally recommended to receive adjuvant chemotherapies following nephroureterectomy in our institution during the study period. Postoperative adjuvant radiotherapy regimens were not routinely used. Patients were assessed by urine cytology and cystoscopy every 3 months for 2 years following nephroureterectomy, every 6 months for the next 3 years, and then every 6 to 12 months thereafter. Computed tomography and either MRI or excretory urography were conducted every 6 months for 5 years and annually thereafter. Disease recurrence was defined as any recurrence documented by radiograph or pathology-proven failure in nonbladder lesions such as contralateral kidney, operative site, regional lymph nodes, or distant metastasis. The cause of death was determined by the treating physicians. The independent variables included in the present study were age, gender, tumor location, pathologic factors (tumor grade, pathologic T stage, and the appearance of LVI), and the status of adjuvant chemotherapy. Tumor location was divided into 2 areas: the renal pelvis or ureter based upon the location of the dominant lesion.

Tissue samples

All the specimens were fixed in 10% formalin and embedded in paraffin. All pathologic specimens were reviewed again by genitourinary pathologists to unify the reproducibility of the diagnosis. As for the pathologic stage, all neoplasms were classified according to the 2002 tumor–node–metastasis staging system. Histologic grades were assigned according to the 3-tiered World Health Organization classification, namely low (G1 and G2) and high (G3) grades. Lymphovascular invasion was defined as the presence of tumor cells within an endothelium-lined space without underlying muscular walls.

Immunohistochemistry

We carried out immunohistochemical staining for VASH1 and CD34 (as a marker of vascular endothelial cells). All the tissue samples were fixed in 10% formalin, embedded in paraffin, and cut into 4-μm thick sections and

Published OnlineFirst June 6, 2012; DOI: 10.1158/1078-0432.CCR-12-0073

placed on silane-coated glass slides. Tissue sections were deparafinized in xylene, and hydrated through graded alcohols and to distilled water. Antigen retrieval was carried out in 10 mmol/L Tris buffer (Dako target retrieval solution pH 9.0, Dako) for VASH1, heated in autoclave at 121°C for 10 minutes. Endogenous peroxidase activity was blocked by 0.3% hydrogen peroxidase/methanol for 20 minutes at room temperature. The tissue sections were then incubated for 15 minutes at room temperature in a blocking solution of 6% dry milk in PBS. After that they were stained for 60 minutes at room temperature with primary antibodies, followed by staining for 30 minutes at room temperature with secondary antibodies. The primary antibodies were all mouse monoclonal antibodies (mAbs): anti-human VASH1 mAb diluted at 1:400 and anti-CD34 (Nichirei Biosciences) diluted at 1:200. We previously described a mouse mAb against a synthetic peptide corresponding to the 286 to 299 amino acid sequence of VASH1 (20). After washing with PBS, the tissue sections were incubated with secondary antibodies against mouse IgG conjugated to a peroxidase-labeled polymer (Histofine Simple Stain MAX PO (M), Nichirei Biosciences) for 30 minutes. Color was developed with 3,3′-diaminobenzamine in 50 mmol/L Tris-HCl (pH 7.5) containing 0.005% hydrogen peroxide. The sections were counterstained with hematoxylin. The positive control slide for CD34 antigen was prepared from paraffin-fixed bladder cancer tissue with high MVD. The appropriate negative control slides for CD34 antigen and VASH1 were prepared by substituting the primary antibody with the immune globulin fraction of nonimmune mouse serum at the same concentration in each staining run.

Evaluation of immunostaining

Two authors independently evaluated immunoreactivity. They were blinded to the clinical course of the patients and the average of the numbers counted by the 2 investigators was used for subsequent analyses. Olympus BH2 (Olympus) was used for the analysis. The number of microvessels was counted within the tumor. Microvessels were identified on the basis of their architecture, lumen lined by endothelial cells, complemented by positivity of the endothelial cells for anti-CD34 after scanning the immunostained section at low magnification (×40 and ×100). The areas with highest number of distinctly highlighted microvessels were selected and counted at high magnification (×200). We evaluated at least 6 areas in high-power fields and selected one area with the highest number of vessels. Any immunostained endothelial cells or clusters separated from adjacent vessels were counted as a single microvessel, even in the absence of vessel lumen. Each single count was defined as the highest number of microvessels identified at the "hot spot" as previously shown (14,23,24). The highest number of microvessels in the hot spot was counted for MVD. VASH1-positive signals were counted in the "hot spot" in which the highest number of vessels positive for anti-CD34 was identified. We regarded the number of VASH1-positive signals per mm^2 as "VASH1 density" (23,25, 26). The median value of MVD and VASH1 density were 67.2 ± 3.8/mm^2 and 39.5 ± 3.3/mm^2, respectively. We used a median MVD ≥70/mm^2 and a VASH1 density ≥40/mm^2, as the cutoff levels.

Statistical analysis

The associations between clinicopathologic parameters and VASH1 density of the tumor were analyzed. These associations were validated by the χ^2 test or Mann–Whitney *U* test. Recurrence-free survival and cancer-specific survival rates were estimated using Kaplan–Meier method and were compared by the log-rank test. Survival time was calculated from the date of operation. Multivariate analysis was conducted using the Cox proportional hazard model with stepwise forward selection. Differences among groups were regarded as significant when $P < 0.05$. These analyses were conducted with the SPSS version 18.0 statistical software package.

Results

Patient characteristics

Table 1 shows the association of clinicopathologic characteristics with MVD or VASH1 density in our study population. The median age of the patients was 68 years (range: 36–89 years). One hundred and thirty-three patients (77.8%) were men. Pathologic analysis revealed 101 patients (59.1%) with tumors in the renal pelvis and 70 patients (40.9%) with tumors in the ureter. Tumor grade was low in 56 cases (32.7%) and high in 115 cases (67.3%). In 106 patients (62.0%), the disease was in ≥pT2 stage; 62 patients (36.3%) were positive for LVI. Cisplatin-based adjuvant chemotherapy was carried out in 28 patients (16.4%). During a median follow-up of 3.8 years, 42 patients (24.6%) experienced tumor recurrence, and of these 34 (19.9%) died of the disease during follow-up.

VASH1 expression in UTUC

To elucidate the biologic significance of VASH1 in UTUC, we examined the immunohistochemical expression of VASH1 in UTUC (Fig. 1). VASH1 staining of vascular endothelial cells was negative or negligible in superficial and low-grade UTUC (Fig. 1B). However, in other UTUCs with similar pathologic stage and tumor grade, strong VASH1 staining was observed in endothelial cells of microvascular vessels in the tumor lesion (Fig. 1D). In invasive UTUC, we observed low VASH1 density in some vessels (Fig. 1F) and high VASH1 density (Fig. 1H) in many. VASH1 staining of vascular endothelial cells was negative or negligible in large-size vessels of the tumor. The median MVD and VASH1 density (counts per mm^2) were 67.2 ± 3.8 and 39.5 ± 3.3 in 171 patients, respectively (Table 1). Patients with high-grade tumors and ≥pT2 had significantly higher levels of VASH1 density. As it has been reported that VASH1 associates with CD34, we also investigated the relationship between VASH1 and CD34 expression. Using the Spearman correlation coefficient test, we detected a significant positive correlation between MVD and VASH1 density in microvessels in the tumor ($\rho = 0.636$, $P < 0.001$).

Published OnlineFirst June 6, 2012; DOI: 10.1158/1078-0432.CCR-12-0073

Table 1. Correlation of clinicopathologic parameters and MVD or VASH1 expression in the 171 study patients

Characteristic	No. of patients (%)	MVD (mean ± SD)	*P*	VASH1 density (mean ± SD)	*P*
Age, y					
<70	99 (57.9)	86.4 ± 56.4	0.532	49.3 ± 48.8	0.733
≥70	72 (42.1)	78.1 ± 41.8		46.3 ± 34.3	
Gender					
Male	133 (77.8)	80.9 ± 52.0	0.135	46.3 ± 44.3	0.110
Female	38 (22.2)	89.9 ± 46.3		54.3 ± 38.9	
Tumor location					
Renal pelvis	101 (59.1)	74.2 ± 40.2	0.034	44.2 ± 35.9	0.515
Ureter	70 (40.9)	95.4 ± 61.2		53.6 ± 51.8	
Tumor grade					
Low	56 (32.7)	75.5 ± 36.3	0.578	37.1 ± 29.2	0.028
High	115 (67.3)	86.9 ± 56.3		53.4 ± 47.8	
Pathologic T stage					
<pT2	65 (38.0)	83.3 ± 60.4	0.494	42.2 ± 51.1	0.003
≥pT2	106 (62.0)	82.7 ± 44.2		51.6 ± 37.4	
Lymphvascular invasion					
Positive	62 (36.3)	84.4 ± 48.9	0.813	52.1 ± 42.5	0.233
Negative	109 (63.7)	82.0 ± 52.1		45.7 ± 43.6	
Adjuvant chemotherapy					
Yes	28 (16.4)	78.4 ± 35.9	0.935	51.9 ± 33.8	0.193
No	143 (83.6)	83.8 ± 53.3		47.2 ± 44.9	

Prognostic significance of VASH1 expression in UTUC patients

We conducted univariate and multivariate analysis to determine the indicators for subsequent tumor recurrence following surgery (Table 2). Univariate analysis revealed that high tumor grade, pT2 or greater, presence of LVI, adjuvant chemotherapy, and high VASH1 density (≥40/mm^2) were significant predictors of tumor recurrence. Multivariate analysis showed that high tumor grade ($P = 0.021$, HR = 4.20), presence of LVI ($P < 0.001$, HR = 5.05), and high VASH1 density ($P = 0.024$, HR = 2.10) were also independent predictors of tumor recurrence.

We next conducted univariate and multivariate analysis to determine the indicators for cancer-specific survival. Univariate analysis showed that high tumor grade, pT2 or greater, presence of LVI, adjuvant chemotherapy, and high VASH1 density were significant predictors of cancer-specific survival. Multivariate analysis confirmed that high tumor grade ($P = 0.030$, HR = 5.10), presence of LVI ($P < 0.001$, HR = 5.72), and high VASH1 density ($P = 0.031$, HR = 2.23) were also independent predictors of cancer-specific survival. Similar results could be obtained using other cutoff values of MVD and VASH1 density, such as MVD ≥ 90 or 80/mm^2 and VASH1 density ≥ 60 or 50/mm^2.

Table 3 shows the association between the level of VASH1 density and clinicopathologic characteristics in 171 patients. High VASH1 density was significantly associated with tumor grade, pathologic T stage, and microvessel number, whereas other characteristics such as patient age, gender, tumor location, LVI, and the status of adjuvant chemotherapy were not significantly different in these 2 groups. The 5-year Kaplan–Meier recurrence-free survival and cancer-specific survival rates were 66.1% and 72.8% in patients with high VASH1 density, compared with 81.0% ($P = 0.017$) and 86.5% ($P = 0.042$) in their counterparts (Fig. 2). High level of MVD was not an independent predictor of tumor recurrence ($P = 0.216$) and cancer-specific survival ($P = 0.473$; Fig. 3A and B).

Risk stratification for UTUC according to prognostic factors, tumor grade, LVI, and VASH1 density

We distributed the patients into 3 different groups according to tumor grade, LVI, and VASH1 density, which were the 3 statistically significant variables found by the multivariate Cox regression analysis (Fig. 3C and D). The relative risk of death could be calculated with the formula, exp(1.434 × grade + 1.619 × LVI + 0.740 × VASH1 density) for recurrence-free survival and exp(1.630 × grade + 1.744 × LVI + 0.800 × VASH1 density) for cancer-specific survival. In this equation, the grade equaled 1 if the tumor grade was high, and it equaled 0 if the tumor grade was low. LVI equaled 1 if LVI was present and 0 if absent. VASH1 density equaled 1 if VASH1 density was ≥40/mm^2 and 0 if <40/mm^2. On the basis of the relative risk of death, patients with UTUC were divided into 3 risk groups: low (relative risk of recurrence and death = 1), intermediate (2.10–21.2 for recurrence-free survival, 2.23–29.2 for cancer-specific survival) and high